THE UNIVERSITY of York

DEPARTMENT OF ARCHAEOLOGY (BIOARCH)
B/S Block, Wentworth Way,
York, YO10 5DD, UK

Telephone: +44 (0)1904 328806 (B/S Block)
Telephone: +44 (0)1904 323962 (Kings Manor)
Fax: +44 (0)1904 323902 (Kings Manor)

BIOARCH

Biomolecular and Microscopic Analysis of Dental Calculus from the New Churchyard, London

Metagenomic, chemical and microscopic analysis of skeletal material from the Crossrail Broadgate Ticket Hall (site code XSM10)

July 2016

Metagenomic (ancient DNA) analysis conducted by Dr Jessica Hendy (jessica@eurotast.eu), and Dr Camilla Speller (camilla.speller@york.ac.uk)

Chemical Analysis conducted by Dr Stephen Buckley, Pharos Research (sb55@york.ac.uk)

Microscopic Analysis conducted by Anita Radini (anita.radini@york.ac.uk)

BioArCh, Department of Archaeology, University of York

Table of Contents

1. Metagenomic (Ancient DNA) Analysis

Laboratory Analysis by Dr Jessica Hendy
Data Analysis and Lab Report Preparation by Dr Camilla Speller

1.1 Metagenomic Summary

Ancient DNA analysis of archaeological dental calculus was conducted on 20 skeletons from the Crossrail Broadgate Ticket Hall (site code XSM10). The skeletons were recovered from the New Churchyard, also known as Bedlam Burial Ground, in use from 1569 until at least the 1730s. DNA was extracted from 20 dental calculus samples as well as from two associated rib samples in the ancient DNA laboratory in the BioArCh centre at the University of York, and subjected to high-throughput metagenomic sequencing. The main goals of the analysis were to assess the overall preservation of microbial DNA within the calculus and determine the potential for more in depth analyses of the oral microbiome. Additional goals were to assess preliminary evidence for periodontal, opportunistic and systemic pathogens within the calculus, and identify putative dietary DNA sequences.

All of the dental calculus samples produced sufficient DNA for analysis, and were subjected to metagenomic sequencing (shotgun sequencing) on an Illumina NextSeq 500 platform. Following quality filtering, between 4.8 and 29.3 million sequences were obtained for each individual. The DNA within the dental calculus samples was dominated by bacteria (average of 97.3% across all 20 samples) with relatively lower percentages of archaeal (0.99%), eukaryotic (1.4%) and viral DNA (0.004%). The metagenomic analysis of the dental calculus sample displayed a microbial composition consistent with an oral microbiome, indicating that the samples were generally well preserved and not systematically contaminated with exogenous DNA from the burial environment. The composition of microbial sequences from the dental calculus was distinct from that recovered from the bone samples, which displayed a microbial composition consistent with soil contamination (as expected).

Pathogenic bacteria detected within the dental calculus DNA were dominated by those species associated with the progression of periodontal disease. The most abundant periodontal pathogens were *Tannerella forsythia, Treponema denticola, Porphyromonas gingivalis,* the so-called ‘red complex’ of oral bacteria, with other periodontal pathogens such as *Filifactor alocis* and *Fusobacterium nucleatum* present at lower frequencies. Opportunistic pathogens (organisms capable of causing disease when the host's resistance is compromised) were also detected. The most abundant opportunistic pathogens were those species which are commonly found within the healthy oral microbiome or respiratory tract, but which may occasionally result in acute

infections in immunocompromised individuals. Examples of such opportunistic pathogens included bacteria such *as Streptococcus pneumoniae*, *Streptococcus pyogenes*, *Haemophilus influenzae* which can cause upper and lower respiratory infections. No evidence for pathogens associated with epidemic diseases such as bubonic plague, tuberculosis, or syphilis was identified within the metagenomic data. Although some DNA sequences from other respiratory diseases (e.g., whooping cough) were recovered from the metagenomic data, these were at extremely low abundance and would require further deep sequencing to conclusively identify these as the causative agents of disease.

Within the eukaryotic DNA isolated from the dental calculus, evidence for endogenous host DNA as well as dietary sources was recovered. Percentages of human DNA within the dental calculus ranged from 0.07-0.81% of the obtained sequences, and within the range expected from previous analyses of dental calculus. Based on the number of sequences matching to the sex chromosomes, the quantity of human DNA was sufficient to predict the biological sex of the individual for 18 of the 20 skeletons; the sex predicted through genetic analysis corresponded with the osteological analysis in 17 of the 18 cases. Putative dietary sequences were identified in extremely low abundance; the most commonly identified dietary DNA evidence was associated with cereals (*Triticum* sp.), although animal sources (pig/boar, cow) and other vegetable and herb sequences were also identified (e.g., onion, cabbage family, rosemary, parsley, etc.).

Overall, the metagenomic screening indicated that the biomolecules within the samples were well preserved with a high potential for further, in-depth analysis.

1.2 Methods and Materials

1.2a Sample Preparation

Samples of dental calculus were removed from the skeletons using sterilised dental picks and stored in individual 2.0 mL eppendorf tubes (Table 1). Two fragments of ribs were also sampled for DNA analysis in order to characterise the microbial composition of the local burial environment.

Table 1.1 Teeth sampled and weight of dental calculus collected from each skeleton

Skeleton ID	Lab ID	Element/Tooth Sampled[a]	Sample weight (mg)
Bone			
5586	XSMB1	rib fragment	87.9
8147	XSMB2	rib fragment	93.2
Calculus			
8223	XSM12	T44, T45: RPM1,2 (mandibular)	14.0
4307	XSM6	T27: LM2 (maxillary)	7.0
175	XSM1	T31: LI1 (mandibular)	14.7
420	XSM3	T26: LM1 (maxillary)	13.4
592	XSM4	T14: RPM1 (maxillary)	19.5
807	XSM5	T42: RI2 (mandibular)	23.9
272	XSM2	T41: RI1 (mandibular)	16.9
5396	XSM8	T33, T34: LC1, PM1 (mandibular)	12.0
8103	XSM11	T26: LM1 (maxillary)	7.9
7982	XSM10	T16: RM1 (maxillary)	19.9
5586	XSM9	T26: LM1 (maxillary)	23.9
5218	XSM7	T31, T41: RI1, LI1 (mandibular)	5.0
8105	XSM17	T23: LC1 (maxillary)	18.9
7162	XSM14	T34: LPM1 (mandibular)	12.0
1616	XSM13	T41: RI1 (mandibular)	21.2
8097	XSM16	T31, T41: LI1, RI1 (mandibular)	13.5
8147	XSM18	T44: RPM1 (mandibular)	14.6
8198	XSM19	T31: LI1 (mandibular)	26.8
8204	XSM20	T42: RI2 (mandibular)	14.5
7589	XSM15	T23: LC1 (maxillary)	6.9

[a] Tooth annotation in both FDI notation and anatomical position; L indicates left quadrant; R indicates right quadrant; I indicates incisor, PM indicates premolar; M indicates molar; numbers indicate tooth position.

1.2b Contamination Controls

Sample preparation and DNA extractions were conducted in the BioArCh ancient DNA laboratory at the University of York, which is located in an isolated building, separate from modern DNA laboratories and post-PCR amplification workspaces. The introduction of contamination into the workspace is minimized by the use of protective clothing, including Tyvek suits, gloves, masks and hairnets. The lab is also equipped with UV filtered ventilation and positive airflow, as well as with dedicated equipment and bench UV lights; countertops and other surfaces in the lab are routinely wiped down with dilute sodium hypochlorite. All reagents and equipment in the ancient DNA laboratory are dedicated solely to the study of degraded DNA. Multiple blank DNA extractions and negative PCR controls are run alongside the ancient samples to identify potential contamination at each stage of the procedure.

1.2c Ancient DNA Extraction

DNA was extracted from the dental calculus and bone samples using a protocol based on Dabney et al. (2013). Samples were extracted in two batches, with two extraction blanks prepared alongside each batch. Samples of dental calculus and bone were UV-sterilized for 1 minute on each side. After crushing to a powder, samples were pre-digested for 5 minutes with 1 mL of 0.5M EDTA to remove possible surface contamination. This pre-digestion supernatant was removed, and a further 1.1 mL of 0.5M EDTA added, and rotated at room temperature for seven days to fully demineralize. Samples were centrifuged at 13,000 RPM for 2 minutes and 1 mL of supernatant transferred into fresh tubes. To the supernatant, 100 µL of Qiagen proteinase K was added and rotated at 37 °C for 24 hours.

Zymo-Spin™ reservoirs were attached to Qiagen MinElute spin columns, the apparatus placed in a 50 mL tube, and 13 mL of Qiagen PB (binding buffer) added to each reservoir. The demineralized, digested supernatant was then transferred into the reservoir and re-suspended. The columns were centrifuged at 4,000 RPM for 4 minutes, rotated 180° then centrifuged again for 2 minutes. MinElute columns were removed from the apparatus, placed into 2 mL collection tubes, and centrifuged at 13,000 RPM for 1 minute. The columns were washed twice with 750 µL of PE, and the DNA was eluted in 60 µL of EB following a five minute incubation step. The DNA extract was quantified via Qubit® 2.0 Fluorometer using a High-Sensitivity DNA Assay;

sufficient quantities of DNA were recovered from all of the dental calculus samples, ranging from 5.4 to 106 ng of DNA per mg of calculus (Table 1.2). This yield of DNA is similar to that observed in other archaeological dental calculus samples (Warinner et al. 2015).

Table 1.2 Yield of DNA from dental calculus and bone samples

Skeleton ID	Sample weight (mg)	Concentration of DNA extract (ng/µL)	DNA yield per mg of calculus (ng)
Bone			
5586	87.9	1.66	1.13
8147	93.2	0.4205	0.27
Calculus			
8223	14.0	16.65	71.36
4307	7.0	3.67	31.46
175	14.7	16.30	66.53
420	13.4	23.75	106.34
592	19.5	14.90	45.85
807	23.9	2.13	5.35
272	16.9	27.20	96.57
5396	12.0	6.18	30.88
8103	7.9	6.32	48.00
7982	19.9	11.75	35.43
5586	23.9	14.65	36.78
5218	5.0	3.86	46.32
8105	18.9	8.58	27.24
7162	12.0	2.135	10.68
1616	21.2	16.8	47.55
8097	13.5	4.195	18.64
8147	14.6	15.95	65.55
8198	26.8	29.3	65.60
8204	14.5	1.505	6.23
7589	6.9	1.525	13.26

1.2d Next-Generation Sequencing

For each DNA extract, double-stranded whole genome shotgun Illumina libraries were prepared using a protocol based on Meyer and Kircher (2010). Each library was built using between 200-

400 ng of DNA. The libraries were constructed using a double-barcoding approach as described in Fortes and Paijman (2015) which serves as an additional means to filter chimeric sequences from the dataset, and thus increase the confidence in assigning the sequences to a particular library. Individual P7 indexes were ligated through an indexing PCR step using a proof-reading taq polymerase (AccuPrime Pfx Supermix) with the following cycling conditions were: 95˚C for 5 minutes, and cycles of (95˚C for 15s, 60˚C for 30s, 68˚C for 30s), and a final extension of 68˚C for 5 min. Optimal cycle numbers for library indexing were determined through the use of quantitative PCR (qPCR) using Fast SYBR (Gansauge and Meyer 2013). Amplified libraries were subsequently purified using Qiagen MinElute spin columns, the size distribution of the amplified libraries was determined using an Agilent 2100 Bioanalyzer. The 20 dental calculus libraries were pooled in equimolar concentration (20 ng each) along with two libraries composed of DNA bone extracts (at 5 ng each), two extraction blank controls (5 ng each) and two library negative controls (5 ng each). The pooled libraries were subjected to paired-end sequencing on a single lane of an Illumina NextSeq500 (v2 chemistry, 2x75 cycles, 400mio output) at the Institute for Biochemistry and Biology at the University of Potsdam.

1.2e Bioinformatic methods

The program *bcl2fastq* v2.15.0.4 was used to demultiplex data and convert the raw sequence BCL files to fastq file formats for downstream analysis. The resulting fastq files were trimmed for adapter and index/barcode sequences using the software *cutadapt* 1.8.3 (Martin 2011). During index trimming, one error in the 8bp barcode sequence was allowed (parameter –e 0.125), and sequences were simultaneously filtered to a minimum phred-scaled quality score of 20.

For the microbial community analysis, forward and reverse sequences for the same dataset were merged using *PEAR* v0.9.6 (Zhang et al. 2014). Merged datasets were parsed via OneCodex, a web-interfaced search engine for genomic data, containing roughly 40,000 whole genomes, and providing rapid microbial identification (www.onecodex.com). The merged files were also searched against the NCBI database GenBank through the BLASTn algorithm (Altschul et al. 1990) and parsed via MEGAN6 (Huson et al. 2016) to identify and quantify sequences assigned to oral, opportunistic and systemic pathogens as well as dietary sources. BLAST (Basic Local Alignment Search Tool) is a widely used bioinformatics research tool that can be used to

compare a query against a database of known sequences (Altschul et al. 1990). Nucleotide BLAST (BLASTn) is used to match nucleotide queries against a database of genomic sequences (McGinnis and Madden 2004); the default database for BLASTn is an edited form of GenBank, a comprehensive collection of all publicly available DNA sequences, presently containing data for over 340,000 named organisms (Agarwala et al. 2016). In order to ensure that only the most robust microbial and dietary identifications were included in the analysis, strict parameters suggested in Warinner et al. (2014) were applied through MEGAN, including a >98% identity threshold and an expected value of 2e-20. The expected value (E-value) threshold describes the number of matches that can be estimated to occur by chance when searching a database of a particular size, with lower E-values representing a more significant match to a database sequence (De Wit et al. 2012).

To analyze the human DNA component of dental calculus, the forward and reverse DNA sequences were mapped to the human genome (GRCh38 assembly) using the *Burrows-Wheeler Alignment* 0.7.5a (Li and Durbin 2009) with the following parameters (-l 1024 -n 0.03 -q 20). The program *Samtools* v1.3.1 was used to remove PCR duplicates and calculate the number of unique sequences mapped to the human genome. The bioinformatic computing script developed by Skoglund et al. (2013) was used to estimate the genetic sex for the individuals. Sex assignment is performed by computing the number of alignments to the Y chromosome as a fraction of the total number of alignments to both sex chromosomes.

To authenticate the obtained sequences, the program *mapDamage2.0* (Ginolhac et al. 2011; Jónsson et al. 2013) was run to identify DNA damage patterns typically associated with degraded DNA within the obtained human DNA datasets. MapDamage assesses the pattern of nucleotide misincorporations (observed as elevated C to T substitution towards the 3' end of the sequence and complementary G to A transitions towards the 5' end) as indicative of authentic ancient DNA template. The human sequences within the dental calculus samples demonstrated damage patterns consistent with authentic ancient DNA.

1.3 Metagenomic Results and Discussion

1.3a Microbial Screening Results

The metagenomic datasets were searched against the NCBI GenBank database to assess the overall taxonomic profile of the samples. Between 319 and 2,409k sequences were identified for each dental calculus sample, with the majority of the DNA assigned to bacteria (average 97.3%), with minimal quantities of eukaryotic (1.4%), archaeal (0.99%) and viral DNA (0.004%) identified within the samples (Table 1.3, Figure 1.1).

Table 1.3 Quantity and taxonomic assignment of sequences identified through NCBI Blastn

Skeleton	Sequences identified (n=)	Bacteria		Archaea		Eukaryota		Viruses	
		n=	%	n=	%	n=	%	n=	%
175	2,409,482	2,362,097	98.03%	2,851	0.12%	29,150	1.21%	137	0.0057%
272	926,431	907,313	97.94%	8,361	0.90%	4,848	0.52%	14	0.0015%
420	675,755	617,288	91.35%	4,947	0.73%	51,333	7.60%	2	0.0003%
592	1,563,054	1,554,889	99.48%	4,883	0.31%	1,097	0.07%	0	0%
807	916,027	904,671	98.76%	2,642	0.29%	6,781	0.74%	28	0.0031%
4307	858,323	847,302	98.72%	47	0.01%	9,198	1.07%	159	0.0185%
5218	1,099,199	1,071,791	97.51%	95	0.01%	25,643	2.33%	1	0.0001%
5396	1,065,399	1,036,472	97.28%	561	0.05%	26,828	2.52%	2	0.0002%
5586	475,526	450,004	94.63%	19,230	4.04%	3,597	0.76%	17	0.0036%
7982	718,341	716,314	99.72%	242	0.03%	290	0.04%	8	0.0011%
8103	1,003,968	986,045	98.21%	3,208	0.32%	15,436	1.54%	10	0.0010%
8223	1,185,757	1,168,070	98.51%	9,760	0.82%	5,435	0.46%	78	0.0066%
1616	1,849,834	1,840,868	99.52%	72	0.00%	4,580	0.25%	14	0.0008%
7162	665,734	655,658	98.49%	5,169	0.78%	3,353	0.50%	6	0.0009%
7589	888,159	883,011	99.42%	1,081	0.12%	2,921	0.33%	1	0.0001%
8097	815,889	808,555	99.10%	1,067	0.13%	449	0.06%	5	0.0006%
8105	719,345	702,718	97.69%	8,532	1.19%	5,751	0.80%	6	0.0008%
8147	319,400	289,542	90.65%	22,581	7.07%	5,591	1.75%	53	0.0166%
8198	1,472,806	1,436,770	97.55%	510	0.03%	32,259	2.19%	207	0.0141%
8204	438,996	432,120	98.43%	4,297	0.98%	1,054	0.24%	1	0.0002%

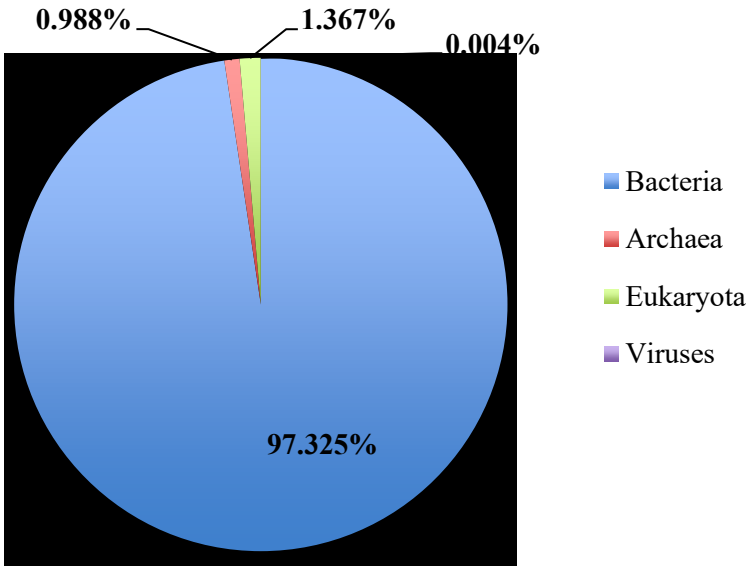

Figure 1.1 Average distribution of broad taxonomic categories from dental calculus sequences identified through NCBI Blastn

The metagenomic data was screened through the genomic search engine OneCodex in order to assess dominant microbial taxa within the calculus samples, and to ascertain the extent to which the metagenomic data was consistent with oral microbial ecology. The dominant microbial phyla within all of the dental calculus samples were consistent with an oral microbiome, dominated by Actinobacteria, Proteobacteria, Firmicutes, Bacteroidetes, Spirochaetes, Chloroflexi, and Synergistetes (Figure 1.2). The proportions of the different phyla were distinct from the bone samples, as well as the blank extractions and laboratory control, which were dominated by Proteobacteria.

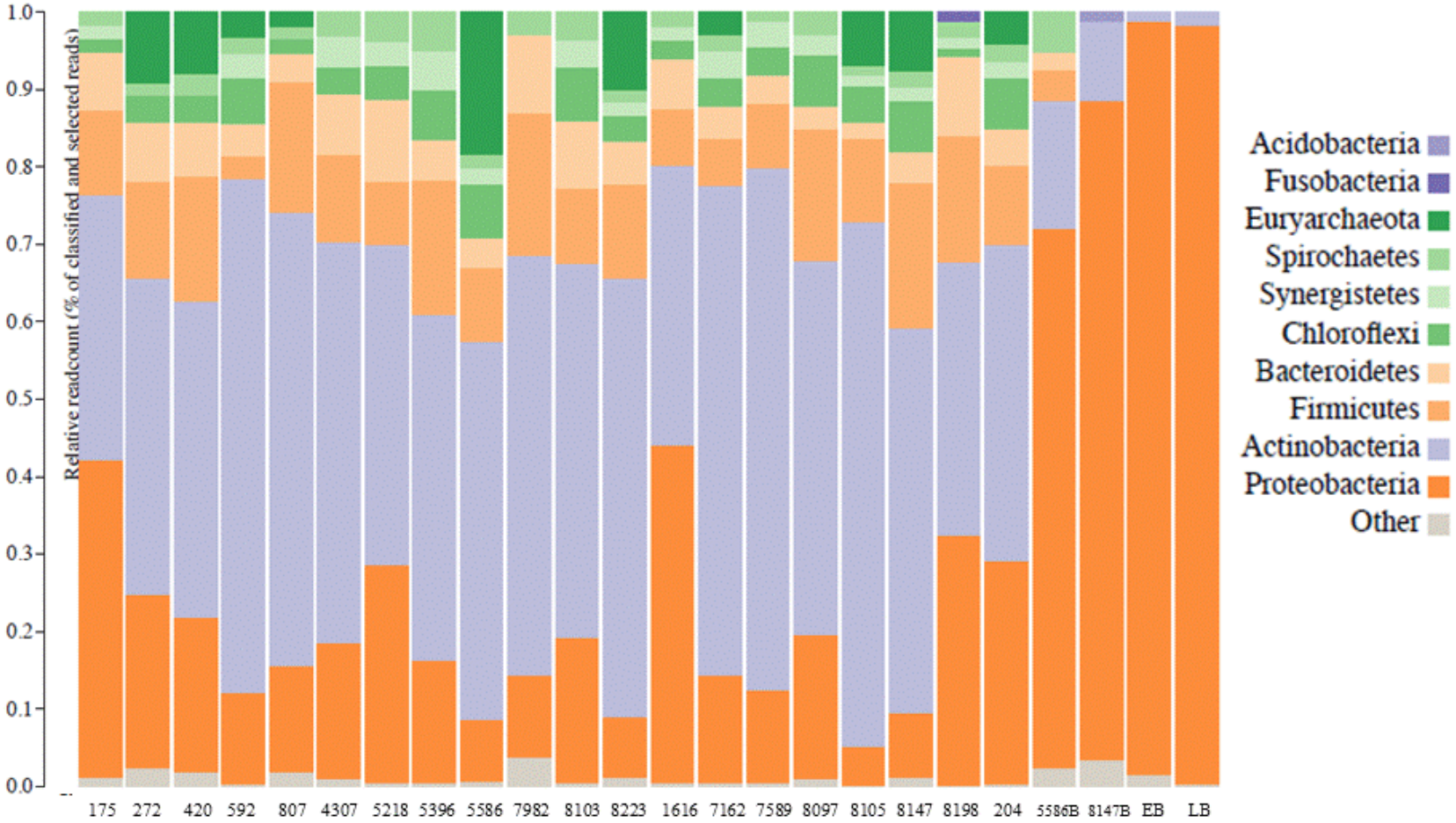

Figure 1.2 Phylum level comparison of dental calculus, bone and laboratory controls. Graph displays relative sequence counts as a percentage of identified sequences; B indicates bone samples, EB indicates Extraction blank control and LB indicates Library blank control.

Within Proteobacteria, the most dominant genera within the dental calculus samples were oral taxa such as *Actinomyces*, *Ottowia*, *Olsenella*, and *Streptococcus*; conversely, within the bone samples and blank controls, the dominant genera were *Bradyrhizobium* (gram-negative soil bacteria), and *Pseudomonas* (widespread in water) both of which are also commonly identified in laboratory consumables (Salter et al. 2014) (Figure 1.3).

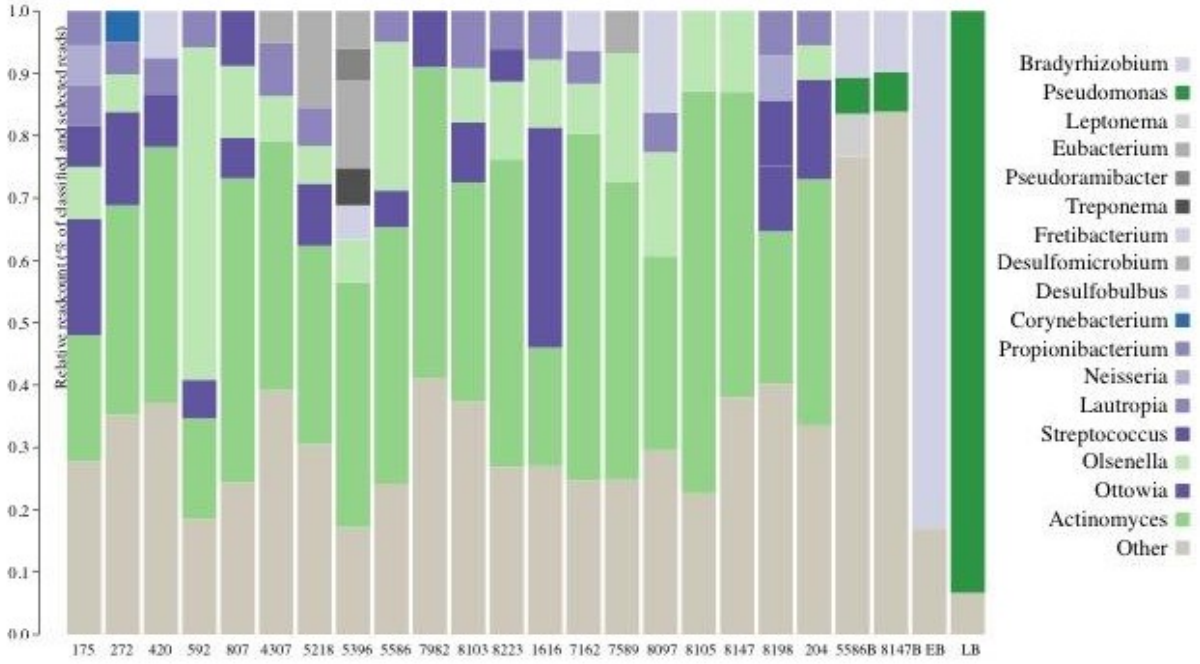

Figure 1.3 Genus level comparison of Proteobacteria within dental calculus, bone and laboratory controls. Graph displays only those genera which contain a minimum of 5% of the identified sequences; B indicates bone samples, EB indicates Extraction blank control and LB indicates Library blank control.

Overall, the metagenomic screening indicated the presence of well-preserved microbial DNA within the dental calculus sample, consistent with the ecology of the oral microbiome, and distinct from bone samples and laboratory controls.

1.3b Pathogen Detection

The metagenomic data was screened against the NCBI database and filtered using MEGAN6 to identify oral, systemic, and opportunistic pathogens. The healthy human oral microbiome includes a number of pathogenic species, which may or may not be actively involved with oral or

systemic disease progression. The most commonly identified pathogenic organisms were bacteria associated with the progression of periodontal disease, in particular the so-called 'red complex' of *Tannerella forsythia*, *Porphyromonas gingivalis* and *Treponema denticola* (Socransky and Haffajee 2005) which were abundant in most dental calculus samples, and consistent with the finding of Warinner et al. (2014) which detected a high abundance of these three pathogens in Medieval individuals from Dalheim, Germany. Other pathogens, now recognised to also be implicated in periodontal disease, such as *Prevotella intermedia*, *Aggregatibacter actinomycetemcomitans*, *Fusobacterium nucleatum*, and *Filifactor alocis* (Aruni et al. 2015) were also present in moderate abundance in some individuals (Figure 1.4).

Opportunistic pathogens such as *Leptotrichia buccalis*, *Olsenella uli*, and *Streptococcus sanguinis* were also observed in moderate abundance. These species are commonly observed within healthy oral microflora, but can cause sepsis, endodontic infections, and bacterial endocarditis, respectively in immunocompromised individuals (Morgenstein et al. 1980; Herzberg et al. 1990). *Neisseria meningitidis* and *Neisseria gonorrhoeae*, the causative agents of bacterial meningitis and gonorrhoea, respectively, were also observed in virtually all skeletons, at varying levels. Both of these *Neisseria* species are obligate human taxa and common members of the human oral microbiome. Opportunistic pathogens implicated in upper and lower bacterial respiratory infections, such as *Streptococcus pneumoniae*, *Streptococcus pyogenes*, *Haemophilus influenzae* were also observed, in lower abundance; respiratory pathogens associated with whooping cough (*Bordetella pertussis*, *Bordetella parapertussis*) were observed within the dataset, but at frequencies of <0.001%, making it difficult to confidently assign the sequences to the species level. No conclusive evidence of epidemic pathogens, such as *Yersinia pestis* (bubonic plague), *Mycobacterium tuberculosis* complex (tuberculosis), or *Treponema pallidum* (syphilis) was identified within the dental calculus datasets.

Further analysis of the dataset may reveal statistically significant differences in pathogen load between individuals, as well as links between osteological and metagenomic indicators of disease (e.g., periodontal disease, respiratory infections).

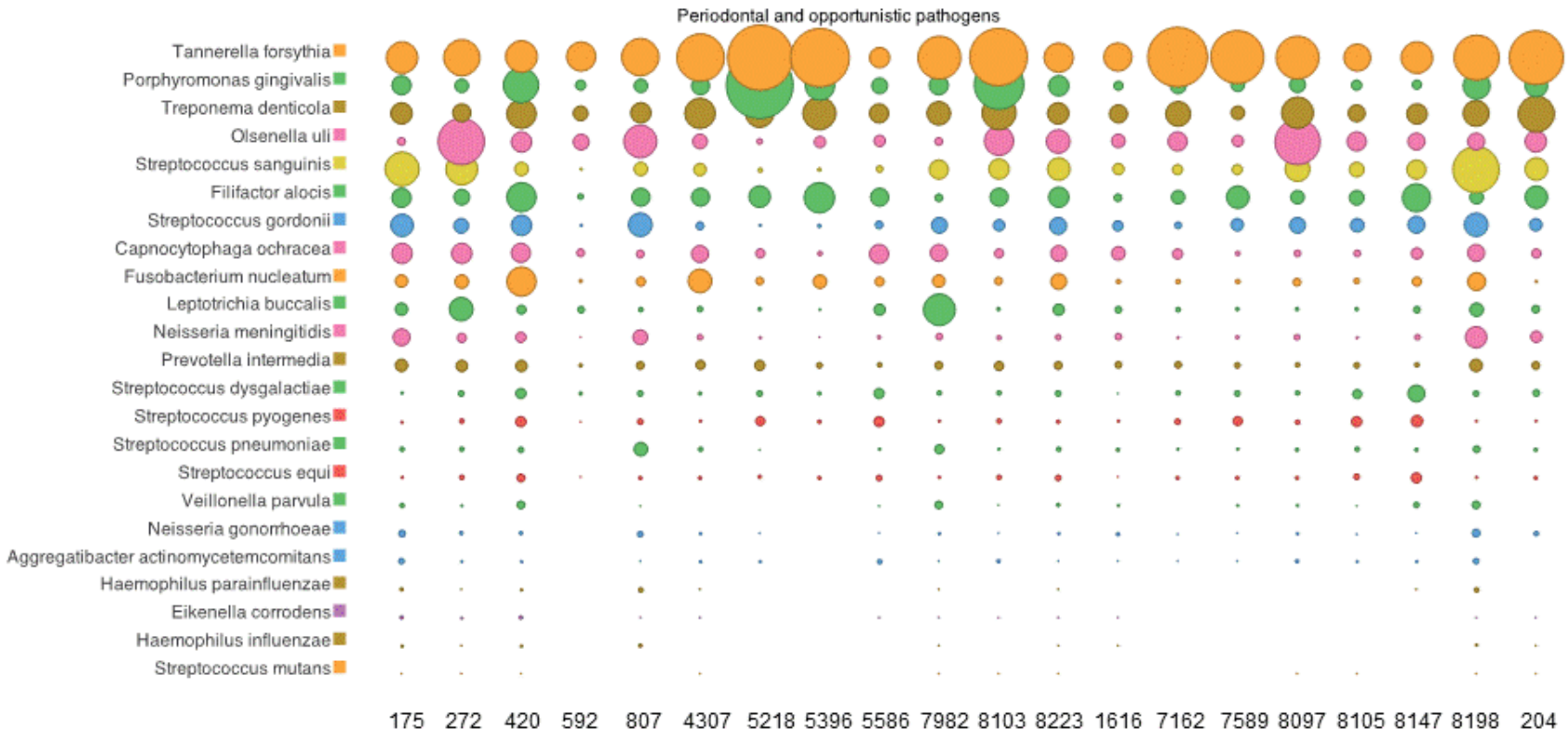

Figure 1.4 Relative abundance of selected periodontal and opportunistic pathogens identified in the dental calculus samples

1.3c Human DNA Analysis Results

The obtained dental calculus and bone DNA sequences were mapped against the human genome to assess the quantity of endogenous human DNA. Between 6,333 and 160,323 sequences aligning to the human genome were obtained from the dental calculus samples, corresponding to 0.07-0.81% endogenous human DNA (Table 1.4). This is similar to percentages of human DNA observed in previous analyses of dental calculus from Medieval Germany (0.5% human DNA) (Warinner et al. 2014) and late prehistoric sites in North America (0.05-0.1% human DNA) (Ozga et al. 2016).

Using a method outlined in Skoglund et al. (2013), the biological sex of the individuals was assessed by quantifying the number of sequences aligning to the X and Y chromosomes. The DNA was sufficiently well preserved to identify the sex of 18 of the 20 individuals, and in all but one case the biological sex predicted by the genetic data was consistent with the osteological identification. Likewise, in two cases where both bone and dental calculus were analysed from the same individuals (skeletons 5586 and 8147), consistent sex identifications were determined from both sets of genetic data. Only in the case of skeleton 8204 did the genetic sex determination (female) and osteological classification (probable male) conflict. However, due to the relatively low percentage of human DNA recovered from this calculus sample (0.08%), the short fragment lengths of the recovered human DNA (average 35.7 bp) as well as the lower confidence interval for the genetic sex prediction, it would be necessary to conduct additional DNA testing on this individual before conclusively assigning a biological sex to the skeleton.

Table 1.4 Human DNA recovered from the dental calculus and bone samples and corresponding genetic and osteological sex identifications

Skeleton	Total Seq	nHuman[a]	% Human DNA	Avg frag length[b]	n_{XY}[c]	n_Y[d]	R_Y[e]	SE	95% CI[f]	Genetic sex assignment	Osteological Sex
175	27,018,328	75,158	0.27%	48.92	1637	12	0.0073	0.0021	0.0032-0.0115	XX	Female
272	22,342,098	49,259	0.22%	42.35	857	13	0.0152	0.0042	0.007-0.0234	Consistent with XX but not XY	Female
420	19,347,516	160,323	0.81%	55.13	4694	39	0.0083	0.0013	0.0057-0.0109	XX	Female
592	26,395,052	17,578	0.07%	33.89	199	5	0.0251	0.0111	0.0034-0.0469	consistent with XX but not XY	Female
807	22,730,308	50,011	0.21%	44.54	888	10	0.0113	0.0035	0.0043-0.0182	consistent with XX but not XY	Female
4307	22,416,110	42,451	0.18%	49.47	869	20	0.023	0.0051	0.013-0.033	consistent with XX but not XY	Female
5218	19,438,416	76,563	0.38%	52.42	1057	73	0.0691	0.0078	0.0538-0.0843	consistent with XY but not XX	Male
5396	10,940,634	44,252	0.40%	59.29	802	65	0.081	0.0096	0.0622-0.0999	consistent with XY but not XX	Male
5586	19,703,522	20,323	0.10%	45.65	220	12	0.0545	0.0153	0.0245-0.0846	consistent with XY but not XX	Male
7982	16,630,991	21,592	0.13%	28.8	136	2	0.0147	0.0103	-0.0055-0.0349	consistent with XX but not XY	Female
8103	22,502,720	54,057	0.24%	52.48	1293	18	0.0139	0.0033	0.0075-0.0203	consistent with XX but not XY	Female
8223	21,938,510	37,390	0.17%	45.02	675	9	0.0133	0.0044	0.0047-0.022	consistent with XX but not XY	Female
1616	27,497,268	42,236	0.15%	40.09	571	4	0.007	0.0035	0.0002-0.0138	XX	Female
7162	29,383,682	58,187	0.19%	36.78	513	25	0.0487	0.0095	0.0301-0.0674	Not Assigned	?Male
7589	24,186,578	47,311	0.19%	37.37	473	16	0.0338	0.0083	0.0175-0.0501	Not Assigned	Male
8097	7,304,884	6,333	0.09%	56.98	102	10	0.098	0.0294	0.0403-0.1557	consistent with XY but not XX	?Male
8105	23,351,036	57,091	0.24%	42.61	569	42	0.0738	0.011	0.0523-0.0953	consistent with XY but not XX	?Male
8147	4,842,098	19,272	0.36%	52.5	262	18	0.0687	0.0156	0.0381-0.0993	consistent with XY but not XX	Male
8198	21,348,412	81,338	0.37%	54.89	1404	134	0.0954	0.0078	0.0801-0.1108	XY	?Male
8204	24,887,268	21,731	0.08%	35.7	225	8	0.0356	0.0123	0.0114-0.0598	consistent with XX but not XY	?Male
5586	15,364,096	529,758	2.70%	57.3	385	37	0.0961	0.015	0.0667-0.1255	consistent with XY but not XX	Male
8147	5,256,328	20,121	0.35%	59.06	348	29	0.0833	0.0148	0.0543-0.1124	consistent with XY but not XX	Male

[a] number of sequences aligning to the human genome; [b] average fragment length of human DNA sequences; [c] number of alignments to both sex chromosomes; [d] number of alignments to the Y chromosome; [e] Ratio of Y chromosome alignments where $R_Y = (n_Y/(n_X + n_Y))$; [f] 95% confidence interval computed by normal approximation as $R_Y \pm 1.96 \times R_Y \times (1 - R_Y)/(n_X + n_Y)$.

1.3d Dietary DNA Results

Previous metagenomic studies of dental calculus identified the presence of dietary DNA sequences, albeit at an extremely low frequency (Warinner et al. 2014). Within the current study, a total of 140 putative dietary sequences were recovered from the 20 studied individuals (Table 1.5). The most common food product identified was cereals (specifically the genus *Triticum*), accounting for 80% of the dietary sequences. Due to the similarities in the nuclear genomes of *T. aestivum* (common wheat or bread wheat), *T. monococcum* (Einkorn wheat), *T. durum* (Durum wheat), and *Aegilops tauschii* (Goatgrass), it is difficult to assign the obtained cereal sequences to particular species within the Triticeae tribe. Thus, the obtained *Triticum* and *Aegilops* species sequences should not be considered 'species specific', but instead indicative of the consumption of Triticum cereals in general. DNA sequences assigned to Brassicaceae (cabbage or mustard family) and onion were identified in two individuals, respectively. DNA evidence of herbs (parsley, rosemary, and *Artemisia* sp.) was identified in two individuals, and DNA sequences specific to grapes (*Vitis vinifera*), the Cucurbit family (which includes gourds, melons and squash) and the Legume family were identified in one individual each. DNA sequences matching to animal products were found in seven individuals, with the most common sequences matching cow and domestic pig/wild boar, as well as DNA sequences matching chicken and goose in one individual each. The fact that no putative dietary sequences were identified within the bone samples or the laboratory controls suggests that the dietary DNA sequences within the dental calculus are not a result of systematic laboratory contamination or sequence misidentification, lending authenticity to the obtained dietary data.

Although the DNA evidence for dietary sources is extremely limited, it provides new evidence for the use of vegetative material such as herbs and leafy greens, which tend not to survive in the archaeological record.

Table 1.5 Dietary DNA sequences identified in the dental calculus samples

Skeleton	Lab code	Species Name	Common name	Number of Sequences
175	XSM1	No dietary sequences identified		
272	XSM2	*Triticum aestivum*	Bread wheat	7
		Aegilops tauschii (likely Triticum sp.)	Cereal species	1
420	XSM3	*Bos taurus*	Cow	1
		Sus scrofa	Pig/boar	1
		Triticum aestivum	Bread wheat	10
592	XSM4	*Aegilops tauschii (likely Triticum sp.)*	Cereal species	4
		Triticum aestivum	Bread wheat	69
		Triticum monococcum	Einkorn wheat	3
807	XSM5	No dietary sequences identified		
4307	XSM6	*Bos taurus*	Cow	1
		Gallus gallus	Chicken	1
		Allium cepa	Onion	1
		Triticum aestivum	Bread wheat	2
5218	XSM7	*Triticum aestivum*	Bread wheat	2
5396	XSM8	*Artemisia sp.*	Herbaceous plant	1
		Rosmarinus officinalis	Rosemary	1
		Triticum aestivum	Bread wheat	1
5586	XSM9	*Bos taurus*	Cow	1
		Triticum aestivum	Bread wheat	2
7982	XSM10	*Triticum sp.*	Wheat	1
		Sus scrofa	pig/boar	1
8103	XSM11	*Triticeae*	Wheat and Barley family	1
		Allium cepa	Onion	1
8223	XSM12	No dietary sequences identified		
1616	XSM13	*Vitis vinifera*	Grape	2
		Faboideae	Legume	1
7162	XSM14	*Triticum aestivum*	Bread wheat	1
7589	XSM15	*Brassicaceae*	Cruciferous vegetable	1

8097	XSM16	*Bos taurus*	Cow	1
8105	XSM17	*Triticum aestivum*	Bread wheat	2
8147	XSM18	*Cucurbitaceae sp.*	Gourd/Squash/Melon	1
		Triticum aestivum	Bread wheat	1
8198	XSM19	*Anser sp.*	Goose	1
		Petroselinum crispum	Parsley	1
		Triticum aestivum	Bread wheat	3
8204	XSM20	*Sus scrofa*	Pig/boar	3
		Brassica sp.	Cruciferous vegetable	1
		Triticum aestivum	Bread wheat	8
5586	XSMB1	No dietary sequences identified		
8147	XSMB2	No dietary sequences identified		

1.4 Metagenomic References

Agarwala, R., Barrett, T., Beck, J., Benson, D.A., Bollin, C., Bolton, E., Bourexis, D., Brister, J.R., Bryant, S.H., Lanese, K., Others, 2016. Database resources of the National Center for Biotechnology Information. *Nucleic Acids Res*. 44, D7–D19.

Altschul, S.F., Gish, W., Miller, W., Myers, E.W., Lipman, D.J., 1990. Basic local alignment search tool. *J. Mol. Biol*. 215, 403–410.

Aruni, A.W., Mishra, A., Dou, Y., Chioma, O., Hamilton, B.N., Fletcher, H.M., 2015. *Filifactor alocis*--a new emerging periodontal pathogen. *Microbes Infect.* 17, 517–530.

Dabney, J., Knapp, M., Glocke, I., Gansauge, M.-T., Weihmann, A., Nickel, B., Valdiosera, C., García, N., Pääbo, S., Arsuaga, J.-L., Meyer, M., 2013. Complete mitochondrial genome sequence of a Middle Pleistocene cave bear reconstructed from ultrashort DNA fragments. *Proc. Natl. Acad. Sci. U. S. A*. 110, 15758–15763.

De Wit, P., Pespeni, M.H., Ladner, J.T., Barshis, D.J., Seneca, F., Jaris, H., Therkildsen, N.O., Morikawa, M., Palumbi, S.R., 2012. The simple fool's guide to population genomics via RNA-Seq: an introduction to high-throughput sequencing data analysis. *Mol. Ecol. Resour*. 12, 1058–1067.

Gansauge, M.-T., Meyer, M., 2013. Single-stranded DNA library preparation for the sequencing of ancient or damaged DNA. *Nat. Protoc*. 8, 737–748.

Ginolhac, A., Rasmussen, M., Gilbert, M.T.P., Willerslev, E., Orlando, L., 2011. mapDamage: testing for damage patterns in ancient DNA sequences. *Bioinformatics* 27, 2153–2155.

Fortes, G. G. & Paijmans, J. L. A. 2015 Analysis of Whole Mitogenomes from Ancient Samples. *Methods Mol. Biol*. 1347, 179–195.

Herzberg, M.C., Gong, K., MacFarlane, G.D., Erickson, P.R., Soberay, A.H., Krebsbach, P.H., Manjula, G., Schilling, K., Bowen, W.H., 1990. Phenotypic characterization of *Streptococcus sanguis* virulence factors associated with bacterial endocarditis. *Infect. Immun*. 58, 515–522.

Huson, D.H., Beier, S., Flade, I., Górska, A., El-Hadidi, M., Mitra, S., Ruscheweyh, H.-J., Tappu, R., 2016. MEGAN Community Edition - Interactive Exploration and Analysis of Large-Scale Microbiome Sequencing Data. *PLoS Comput. Biol*. 12, e1004957.

Jónsson, H., Ginolhac, A., Schubert, M., Johnson, P.L.F., Orlando, L., 2013. mapDamage2.0: fast approximate Bayesian estimates of ancient DNA damage parameters. *Bioinformatics* 29, 1682–1684.

Li, H., Durbin, R., 2009. Fast and accurate short read alignment with Burrows-Wheeler transform. *Bioinformatics* 25, 1754–1760.

Martin, M. 2011 Cutadapt removes adapter sequences from high-throughput sequencing reads. *EMBnet.journal* 17, 10–12.

McGinnis, S., Madden, T.L., 2004. BLAST: at the core of a powerful and diverse set of sequence analysis tools. *Nucleic Acids Res*. 32, W20–5.

Meyer, M., Kircher, M., 2010. Illumina sequencing library preparation for highly multiplexed target capture and sequencing. *Cold Spring Harb. Protoc*. 2010, db.prot5448.

Morgenstein, A.A., Citron, D.M., Orisek, B., Finegold, S.M., 1980. Serious infection with *Leptotrichia buccalis*. *Am. J. Med*. 69, 782–785.

Ozga, A.T., Nieves-Colón, M.A., Honap, T.P., Sankaranarayanan, K., Hofman, C.A., Milner, G.R., Lewis, C.M., Stone, A.C., Warinner, C., 2016. Successful enrichment and recovery of whole mitochondrial genomes from ancient human dental calculus. *Am. J. Phys. Anthropol.* doi:10.1002/ajpa.22960

Salter, S.J., Cox, M.J., Turek, E.M., Calus, S.T., Cookson, W.O., Moffatt, M.F., Turner, P., Parkhill, J., Loman, N.J., Walker, A.W., 2014. Reagent and laboratory contamination can critically impact sequence-based microbiome analyses. *BMC Biol*. 12, 87.

Skoglund, P., Storå, J., Götherström, A., Jakobsson, M., 2013. Accurate sex identification of ancient human remains using DNA shotgun sequencing. *J. Archaeol. Sci.* 40, 4477–4482.

Socransky, S.S., Haffajee, A.D., 2005. Periodontal microbial ecology. *Periodontol*. 2000 38, 135–187.

Warinner, C., Rodrigues, J.F.M., Vyas, R., Trachsel, C., Shved, N., Grossmann, J., Radini, A., Hancock, Y., Tito, R.Y., Fiddyment, S., Speller, C., Hendy, J., Charlton, S., Luder, H.U., Salazar-García, D.C., Eppler, E., Seiler, R., Hansen, L.H., Castruita, J.A.S., Barkow-Oesterreicher, S., Teoh, K.Y., Kelstrup, C.D., Olsen, J.V., Nanni, P., Kawai, T., Willerslev, E., von Mering, C., Lewis, C.M., Jr, Collins, M.J., Gilbert, M.T.P., Rühli, F., Cappellini, E., 2014. *Pathogens and host immunity in the ancient human oral cavity*. Nat. Genet. 46, 336–344.

Warinner, C., Speller, C., Collins, M.J., 2015. A new era in palaeomicrobiology: prospects for ancient dental calculus as a long-term record of the human oral microbiome. *Philos. Trans. R. Soc. Lond. B Biol. Sci.* 370. doi:10.1098/rstb.2013.0376

Zhang, J., Kobert, K., Flouri, T., Stamatakis, A., 2014. PEAR: a fast and accurate Illumina Paired-End reAd mergeR. *Bioinformatics* 30, 614–620

2. Chemical analysis using gas chromatography-mass spectrometry

Laboratory analysis carried out by Dr Stephen Buckley, Pharos Research

Data analysis and report prepared by Dr Stephen Buckley, Pharos Research

2.1 Chemical Analysis Introduction

Ten samples of dental calculus taken from ten individuals from New Churchyard, Broadgate, London (XSM10) were analysed by sequential thermal desorption-gas chromatography-mass spectrometry (TD-GC-MS) and pyrolysis-gas chromatography-mass spectrometry (Py-GC-MS). This technique facilitates the identification of both free/unbound and bound/polymeric organic components. From previous analyses of dental calculus samples from similar archaeological contexts, and the analyses of two of the samples presented here, no free organic constituents were or could be expected to be detected apart from minor amounts of carbon dioxide indicative of an oxidised organic component. From the Py-GC-MS analyses of these calculus samples four produced very little organic material, while six samples produced a moderate abundance of organic constituents.

Skeleton 7982 Female 18-25 years from mass burial pit (calculus: 1.85 mg)

The thermal desorption total ion chromatogram (TIC) revealed carbon dioxide and 1(?)-butene as the only detectable components, indicating the virtual absence of free, thermally extractable organic components in this sample. It should be noted, however, that highly polar material could have been present, which would not have successfully eluted from the column, or indeed volatilised sufficiently in the probe. It is not possible to determine the significance of the carbon dioxide and the C_4 alkene, beyond it being indicative of oxidised organic material.

The pyrolysate TIC revealed carbon dioxide as the only detectable component, indicating the essential absence of organic material in this sample. It should be noted, however, that highly polar material could have been present, which would not have successfully eluted from the column, or indeed volatilised sufficiently in the probe. It is not possible to determine the significance of the carbon dioxide, beyond it being indicative of highly oxidised organic material.

Skeleton 8103 Female 18-25 years from mass burial pit (calculus: 1.21 mg)

The thermal desorption total ion chromatogram (TIC) revealed carbon dioxide as the only detectable component, indicating the virtual absence of free, thermally extractable organic

components in this sample. It should be noted, however, that highly polar material could have been present, which would not have successfully eluted from the column, or indeed volatilised sufficiently in the probe. It is not possible to determine the significance of the carbon dioxide, beyond it being indicative of oxidised organic material.

The pyrolysate TIC revealed carbon dioxide as the only significant detectable component, indicating the essential absence of organic material in this sample. A C_7 alkene was also detected as a very minor component, but no other organic compounds were observed. It should be noted, however, that highly polar material could have been present, which would not have successfully eluted from the column, or indeed volatilised sufficiently in the probe. It is not possible to determine the significance of the carbon dioxide, beyond it being indicative of highly oxidised organic material.

Skeleton 8223 Female 18-25 years from mass burial pit (calculus: 1.44 mg)

The pyrolysis-GC-MS TIC revealed carbon dioxide as the major component, with minor amounts of alkenes and alkanes (Fig. 2.1). These included a C_6 alkene, C_6 *n*-1-alkene, C_6 *n*-alkanes and a C_7 alkene. More unusually, a series of C_{11} to C_{15} branched alkanes were also detected as minor components, although their presumed bacterial origin differs to that of the branched hydrocarbons observed in other samples in this study (see below). Benzene was also identified, but no other organic compounds were observed. It should be noted, however, that highly polar material could have been present, which would not have successfully eluted from the column, or indeed volatilised sufficiently in the probe. The carbon dioxide is indicative of highly oxidised organic material in this sample.

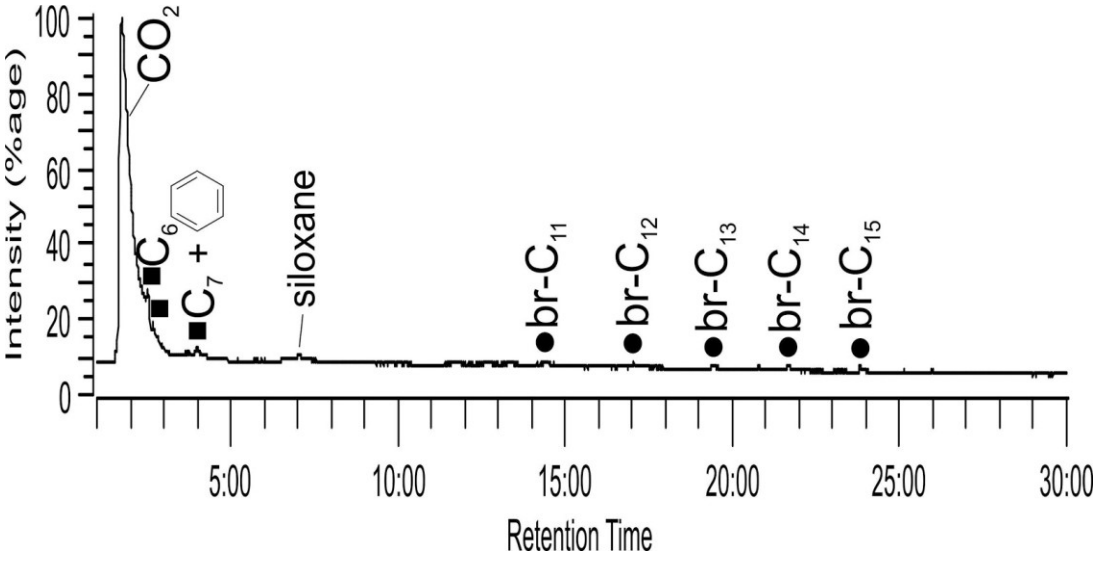

Figure 2.1 Reconstructed total ion chromatogram of the pyrogram (pyrolysis profile) (610 °C for 10s) of sample 8223. Key to Fig. 2.1: Peak identities (x indicates carbon chain length): filled squares, Cx indicates alkenes; filled circles, Cx indicates alkanes (br indicates non-specific branched chain hydrocarbons). Also shown is the structure of benzene. CO_2 indicates carbon dioxide and a siloxane deriving from the GC column is also shown.

Skeleton 4307 Female 26-35 years control sample (calculus: 2.23 mg)

The pyrolysis-GC-MS TIC revealed carbon dioxide as the major component, with moderate amounts of alkenes and alkanes (Fig. 2.2). These were dominated by C_7 to C_{20} n-1-alkenes and n-alkanes, typical of unsaturated and saturated fat/oil-derived acyl lipids (Buckley et al., 1999; Hardy et al., 2012). These provide molecular evidence for a polymeric/bound acyl lipid source. However, in addition to n-1-alkenes and n-alkanes, typical of fat/oil derived lipids, the pyrogram also displayed a series of C_{10} to C_{18} 2-methyl n-1-alkenes and 2-methyl n-alkanes, presumably deriving from the branched fatty acids which are significant components of bacterial triglycerides.

There were components identified in the pyrolysate TIC which can be indicative of proteinaceous material (Hardy et al., 2012; Simmonds, 1970). These include toluene, styrene and benzenepropaneonitrile, although the presence of bacterial markers means the possibility that at least a partial origin could be microbial cannot be excluded. However, taken together, the presence of toluene, styrene and benzenepropanenitrile indicate a protein component which includes amino acids with an aromatic ring such as phenylalanine and tryptophan (Stankiewicz et

al., 1997, 1996) . This is also corroborated by the presence of aliphatic nitriles (carbon numbers $C_{16:0}$ (max) and $C_{18:0}$) suggesting a lipid (fat/oil) in this sample which has combined with protein-derived nitrogen to produce these moieties (Buckley et al., 1999). The presence of carbon dioxide is also consistent with both a lipid and amino acid/protein component in this sample. These findings revealed no polysaccharide markers or higher alkyl aromatics typically observed in soils (Fuentes et al., 2010) . Despite the use of mass chromatograms specifically searching for nicotine and polynuclear aromatic hydrocarbons (PAHs) (the latter group of compounds indicative of combustion processes) these were not detected. It is possible that SIM monitoring specifically for nicotine and PAHs may detect their presence as very minor/trace constituents in future studies.

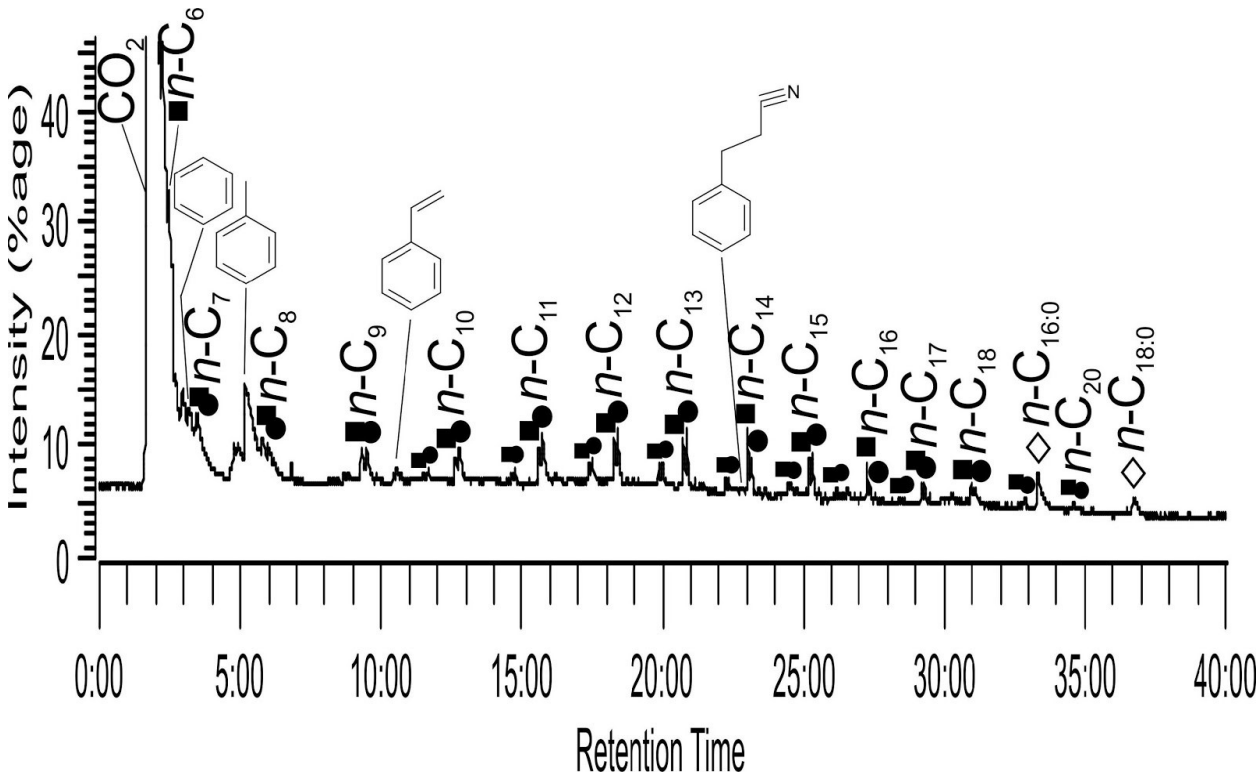

Figure 2.2 Reconstructed total ion chromatogram of the pyrogram (pyrolysis profile) (610 °C for 10s) of sample 4307. Key to Fig. 2.2: Peak identities (x indicates carbon chain length): filled squares, Cx indicates alkenes; filled circles, Cx indicates alkanes; open diamonds, Cx:y indicates acyclic nitriles). Also shown are the structures of four aromatic compounds identified: benzene, toluene, styrene and benzenepropanenitrile. CO_2 indicates carbon dioxide.

Skeleton 175 Female 36-45 years control sample (calculus: 4.08 mg)

The pyrolysis-GC-MS TIC revealed carbon dioxide as the major component, with significant amounts of alkenes and alkanes (Fig. 2.3). These were dominated by C_7 to C_{22} *n*-1-alkenes and *n*-alkanes, typical of unsaturated and saturated fat/oil-derived acyl lipids (Buckley et al., 1999; Hardy et al., 2012) . These provide molecular evidence for a polymeric/bound acyl lipid source. However, in addition to *n*-1-alkenes and *n*-alkanes, typical of fat/oil derived lipids, the pyrogram also displayed a series of C_9 to C_{18} 2-methyl *n*-1-alkenes and 2-methyl *n*-alkanes, presumably deriving from the branched fatty acids which are significant components of bacterial triglycerides.

There were components identified in the pyrolysate TIC which can be indicative of proteinaceous material (Hardy et al., 2012; Simmonds, 1970). These include toluene, styrene, pyridine, pyrrole, C_1 and C_2 alkyl pyrroles, benzyl nitrile (phenylacetonitrile), benzenepropanenitrile, indole and 3-methylindole (skatole) (Hardy et al., 2012; Simmonds, 1970) identified this is likely to be the main origin of these compounds in this sample, suggesting to an appreciable protein-derived component (Hardy et al., 2012; McCobb et al., 2001) , although the presence of bacterial markers means the possibility that at least a partial origin could be microbial cannot be excluded. However, taken together, the presence of toluene, styrene and benzyl nitrile can indicate the amino acid phenylalanine (Stankiewicz et al., 1997, 1996) . In addition, indole and 3-methylindole (skatole) are consistent with a tryptophan amino acid source (Simmonds, 1970; Stankiewicz et al., 1997, 1996). This is also corroborated by the presence of aliphatic nitriles (carbon numbers *n*-$C_{6:1}$, *n*-$C_{13:0}$, *n*-$C_{14:0}$, *i*-$C_{15:0}$, *i*-$C_{16:0}$, *n*-$C_{16:1}$, *n*-$C_{16:0}$ (max), *i*-$C_{17:0}$, a*i*-$C_{17:0}$, *n*-$C_{17:0}$, $C_{18:1}$ (x2 isomers) and $C_{18:0}$) suggesting a lipid (fat/oil) in this sample which has combined with protein-derived nitrogen to produce these moieties (Buckley et al., 1999), although the branched constituents may suggest a microbial source, at least in part. The presence of carbon dioxide is also consistent with both a lipid and amino acid/protein component in this sample. These findings revealed no polysaccharide markers or higher alkyl aromatics typically observed in soils (Fuentes et al., 2010). Despite the use of mass chromatograms specifically searching for nicotine and polynuclear aromatic hydrocarbons (PAHs) (the latter group of compounds indicative of combustion processes) these were not detected. It is possible

that SIM monitoring specifically for nicotine and PAHs may detect their presence as very minor/trace constituents in future studies.

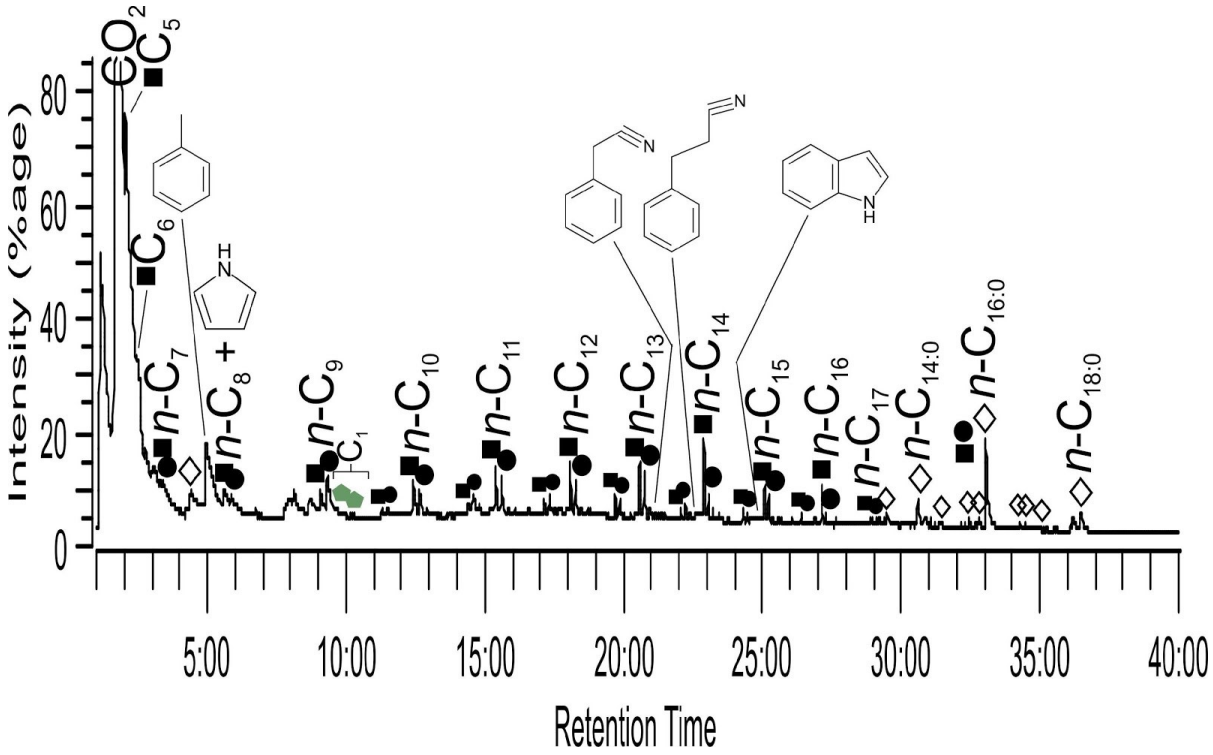

Figure 2.3 Reconstructed total ion chromatogram of the pyrogram (pyrolysis profile) (610 °C for 10s) of sample 175. Key to Fig. 2.3: Peak identities (x indicates carbon chain length): filled squares, Cx indicates alkenes; filled circles, Cx indicates alkanes; open diamonds, Cx:y indicates acyclic nitriles; green filled pentagons indicates alkyl pyrroles (with alkyl chain length above, Cx). Also shown are the structures of five aromatic compounds identified: toluene, pyrrole, benzyl nitrile, benzenepropanenitrile and indole. CO_2 indicates carbon dioxide.

Skeleton 8097 ?Male adult from mass burial pit (calculus: 1.02 mg)

The pyrolysis-GC-MS TIC revealed carbon dioxide as the only significant detectable component, indicating the absence of non-oxidised organic material in this sample. A C_6 alkene, cyclopentadiene and benzene were also detected as minor components, but no other organic compounds were observed. It should be noted, however, that highly polar material could have been present, which would not have successfully eluted from the column, or indeed volatilised sufficiently in the probe. It is not possible to determine the significance of the carbon dioxide, beyond it being indicative of highly oxidised organic material.

Skeleton 8147 Male 26-35 years from mass burial pit (calculus: 1.41 mg)

The pyrolysis-GC-MS TIC revealed carbon dioxide as the major component, with moderate amounts of alkenes and alkanes (Fig. 2.4). These were dominated by C_7 to C_{19} *n*-1-alkenes and *n*-alkanes, typical of unsaturated and saturated fat/oil-derived acyl lipids (Buckley et al., 1999; Hardy et al., 2012). These provide molecular evidence for a polymeric/bound acyl lipid source. However, in addition to *n*-1-alkenes and *n*-alkanes, typical of fat/oil derived lipids, the pyrogram also displayed a series of C_{11} to C_{16} 2-methyl *n*-1-alkenes and 2-methyl *n*-alkanes, presumably deriving from the branched fatty acids which are significant components of bacterial triglycerides.

There were components identified in the pyrolysate TIC which can be indicative of proteinaceous material (Hardy et al., 2012; Simmonds, 1970). These include toluene, styrene, C_2 alkyl pyrroles and benzenepropaneonitrile (trace), although the presence of bacterial markers means the possibility that at least a partial origin could be microbial cannot be excluded. However, taken together, the presence of toluene, styrene and benzenepropanenitrile indicate a protein component which includes amino acids with an aromatic ring such as phenylalanine and tryptophan (Stankiewicz et al., 1997, 1996). This is also corroborated by the presence of aliphatic nitriles (carbon numbers *i*-$C_{15:0}$, *n*-$C_{16:0}$ (max), *i*-$C_{17:0}$, *n*-$C_{18:1}$ (x2 isomers) and *n*-$C_{18:0}$) suggesting a lipid (fat/oil) in this sample which has combined with protein-derived nitrogen to produce these moieties(Buckley et al., 1999), although the branched constituents may suggest a microbial source, at least in part. The presence of carbon dioxide is also consistent with both a lipid and amino acid/protein component in this sample. These findings revealed no polysaccharide markers or higher alkyl aromatics typically observed in soils (Fuentes et al., 2010). Despite the use of mass chromatograms specifically searching for nicotine and polynuclear aromatic hydrocarbons (PAHs) (the latter group of compounds indicative of combustion processes) these were not detected. It is possible that SIM monitoring specifically for nicotine and PAHs may detect their presence as very minor/trace constituents in future studies.

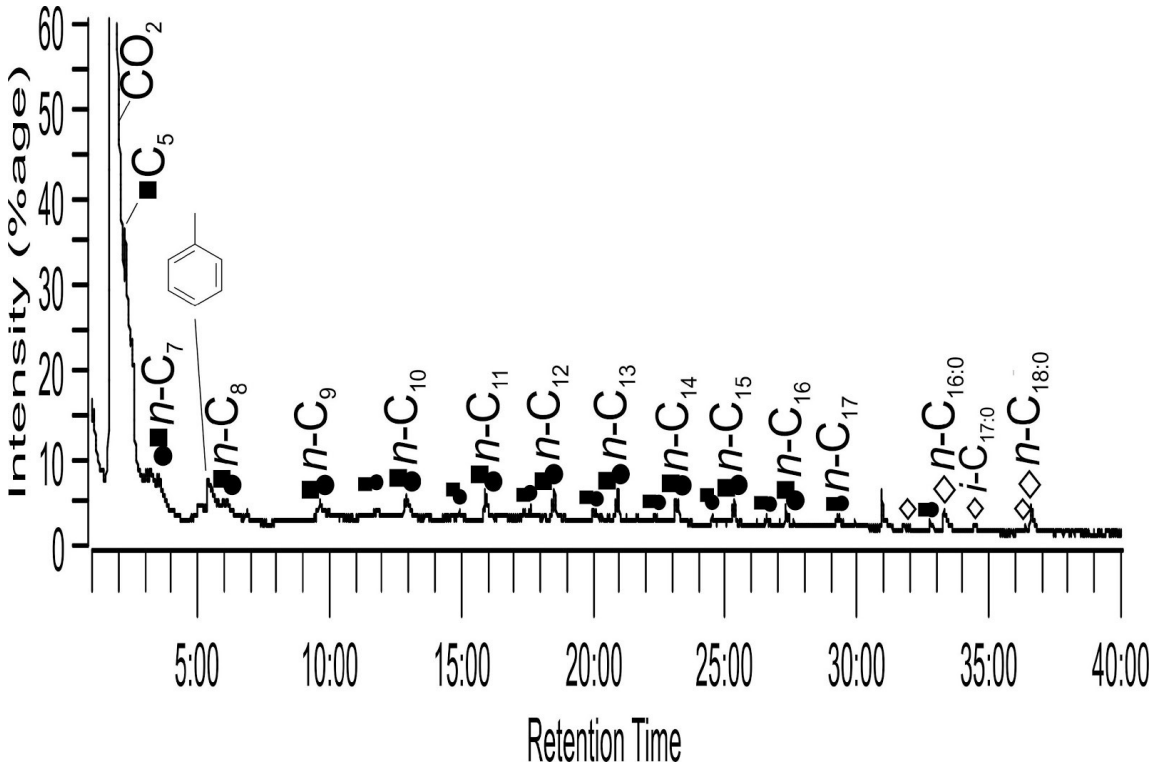

Figure 2.4 Reconstructed total ion chromatogram of the pyrogram (pyrolysis profile) (610 °C for 10s) of sample 8147. Key to Fig. 2.4: Peak identities (x indicates carbon chain length): filled squares, Cx indicates alkenes; filled circles, Cx indicates alkanes; open diamonds, Cx:y indicates acyclic nitriles. Also shown is the structures of toluene. CO_2 indicates carbon dioxide.

Skeleton 5218 Male 36-45 years control sample (calculus: 3.17 mg)

The pyrolysis-GC-MS TIC revealed carbon dioxide as the major component, with moderate amounts of alkenes and alkanes (Fig. 2.5). These were dominated by C_9 to C_{20} *n*-1-alkenes and *n*-alkanes, typical of unsaturated and saturated fat/oil-derived acyl lipids (Buckley et al., 1999; Hardy et al., 2012). These provide molecular evidence for a polymeric/bound acyl lipid source. However, in addition to *n*-1-alkenes and *n*-alkanes, typical of fat/oil derived lipids, the pyrogram also displayed a series of C_{11} to C_{16} 2-methyl *n*-1-alkenes and 2-methyl *n*-alkanes, presumably deriving from the branched fatty acids which are significant components of bacterial triglycerides.

There were components identified in the pyrolysate TIC which can be indicative of proteinaceous material (Hardy et al., 2012; Simmonds, 1970). These include toluene, styrene, pyridine, pyrrole, C_1 alkyl pyrroles, benzenepropaneonitrile and indole, although the presence of

bacterial markers means the possibility that at least a partial origin could be microbial cannot be excluded. However, taken together, the presence of toluene, styrene and benzenepropanenitrile indicate a protein component which includes amino acids with an aromatic ring such as phenylalanine and tryptophan (Stankiewicz et al., 1997, 1996). In addition, the presence of indole is consistent with a tryptophan amino acid source (Fuentes et al., 2010; Stankiewicz et al., 1997, 1996). This is also corroborated by the presence of aliphatic nitriles (carbon numbers *n*-$C_{13:0}$, *n*-$C_{14:0}$, *n*-$C_{16:0}$ (max) and *n*-$C_{18:0}$) suggesting a lipid (fat/oil) in this sample which has combined with protein-derived nitrogen to produce these moieties (Buckley et al., 1999). The presence of carbon dioxide is also consistent with both a lipid and amino acid/protein component in this sample. The thermally-derived carbohydrate markers 2-methyl-2-cyclopenten-1-one and 2,3-dimethyl-2-cyclopenten-1one were identified as minor constituents and are indicative of the original polymeric carbohydrate source (e.g. starch) (McCobb et al., 2001). No higher alkyl aromatics typically observed in soils were detected ((Fuentes et al., 2010) . Despite the use of mass chromatograms specifically searching for nicotine and polynuclear aromatic hydrocarbons (PAHs) (the latter group of compounds indicative of combustion processes) these were not detected. It is possible that SIM monitoring specifically for nicotine and PAHs may detect their presence as very minor/trace constituents in future studies.

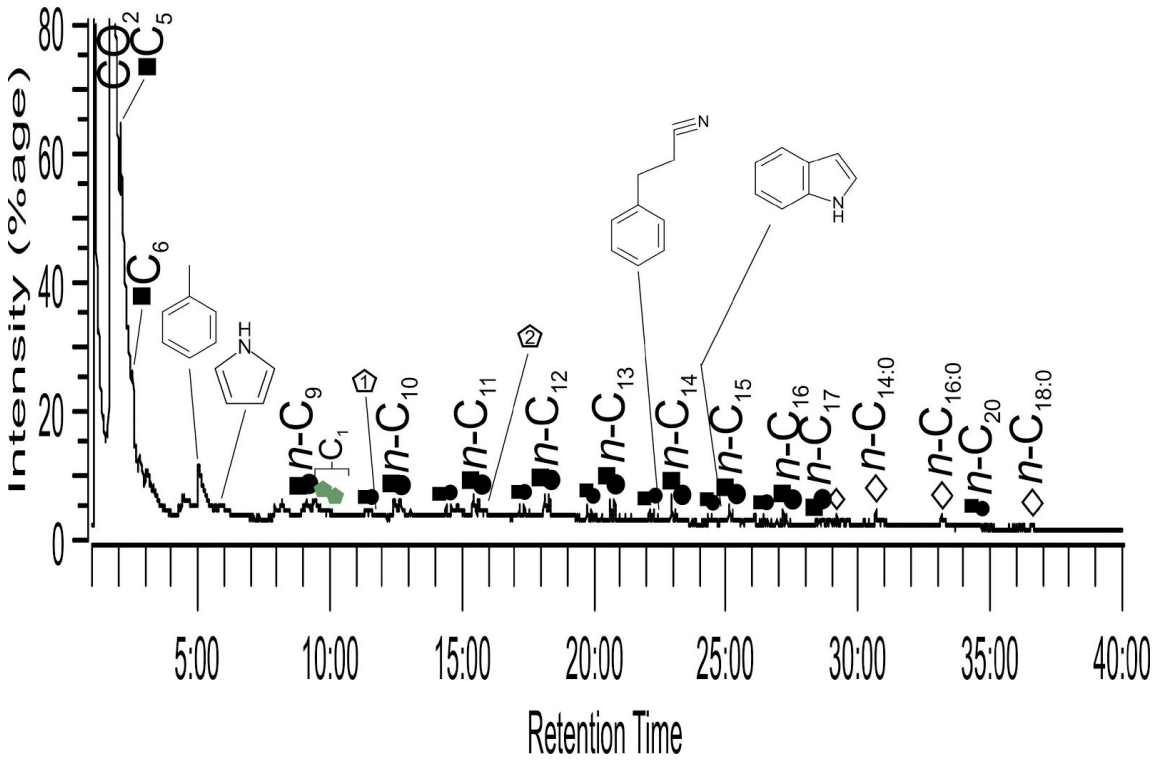

Figure 2.5 Reconstructed total ion chromatogram of the pyrogram (pyrolysis profile) (610 °C for 10s) of sample 5218. Key to Fig. 2.5: Peak identities (x indicates carbon chain length): filled squares, Cx indicates alkenes; filled circles, Cx indicates alkanes; open diamonds, Cx:y indicates acyclic nitriles; green filled pentagons indicates alkyl pyrroles (with alkyl chain length above, Cx); open pentagons with numerals inside indicates carbohydrate pyrolysis markers, 1 is 2-methyl-2-cyclopenten-1-one and 2 is 2,3-dimethyl-2-cyclopentene-1-one. Also shown are the structures of four aromatic compounds identified: toluene, pyrrole, benzenepropanenitrile and indole. CO_2 indicates carbon dioxide.

Skeleton 5396 Male 26-35 years control sample (calculus: 0.92 mg)

The pyrolysis-GC-MS TIC revealed carbon dioxide as the major component, with moderate amounts of alkenes and alkanes (Fig. 2.6). These were dominated by C_7 to C_{18} *n*-1-alkenes and *n*-alkanes, typical of unsaturated and saturated fat/oil-derived acyl lipids (Buckley et al., 1999; Hardy et al., 2012). These provide molecular evidence for a polymeric/bound acyl lipid source. However, in addition to *n*-1-alkenes and *n*-alkanes, typical of fat/oil derived lipids, the pyrogram also displayed a series of C_{10} to C_{16} 2-methyl *n*-1-alkenes and 2-methyl *n*-alkanes, presumably deriving from the branched fatty acids which are significant components of bacterial triglycerides.

There were components identified in the pyrolysate TIC which can be indicative of proteinaceous material (Hardy et al., 2012; Simmonds, 1970). These include toluene, although

the presence of bacterial markers means the possibility that at least a partial origin could be microbial cannot be excluded. However, this is also corroborated by the presence of aliphatic nitriles (carbon numbers $C_{16:0}$ (max) and $C_{18:0}$) suggesting a lipid (fat/oil) in this sample which has combined with protein-derived nitrogen to produce these moieties (Buckley et al., 1999). The presence of carbon dioxide is also consistent with both a lipid and amino acid/protein component in this sample. These findings revealed no polysaccharide markers or higher alkyl aromatics typically observed in soils (Fuentes et al., 2010). Despite the use of mass chromatograms specifically searching for nicotine and polynuclear aromatic hydrocarbons (PAHs) (the latter group of compounds indicative of combustion processes) these were not detected. It is possible that SIM monitoring specifically for nicotine and PAHs may detect their presence as very minor/trace constituents in future studies.

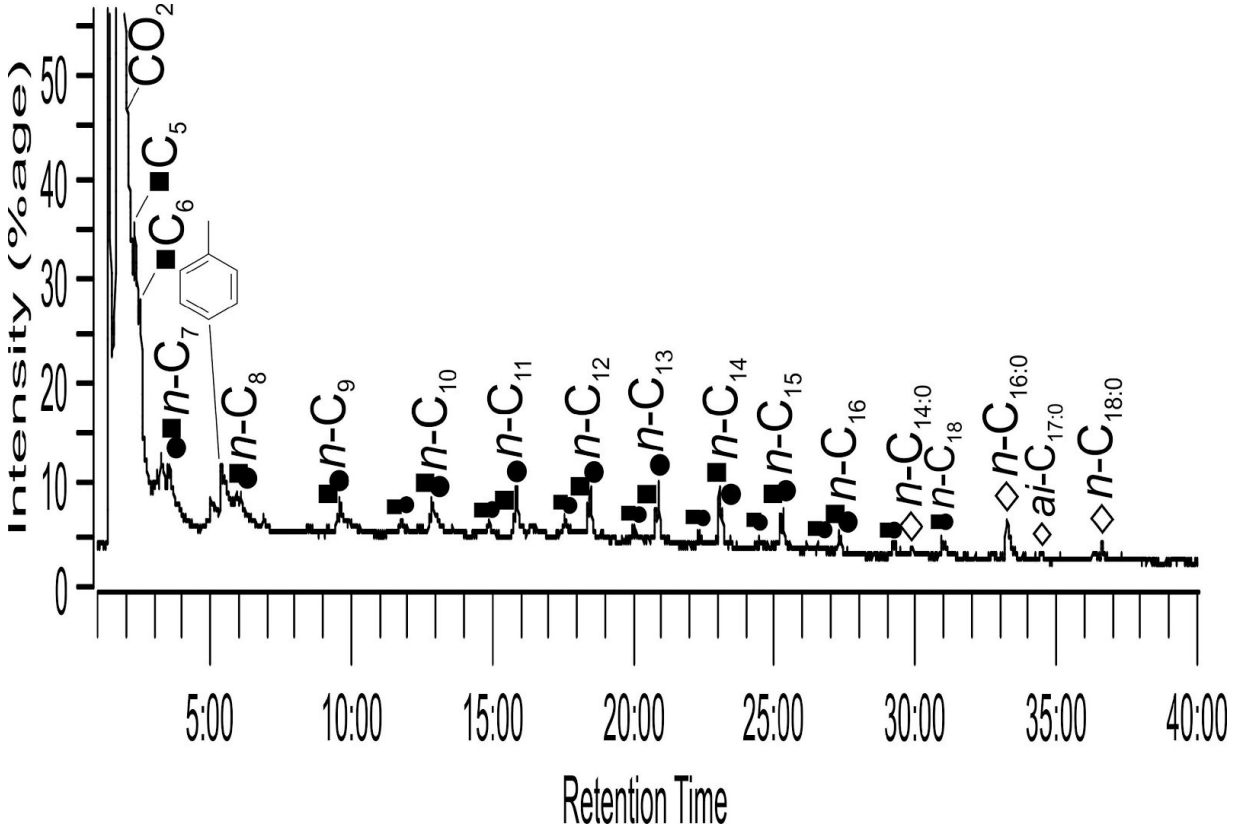

Figure 2.6 Reconstructed total ion chromatogram of the pyrogram (pyrolysis profile) (610 °C for 10s) of sample 5396. Key to Fig. 2.6: Peak identities (x indicates carbon chain length): filled squares, Cx indicates alkenes; filled circles, Cx indicates alkanes; open diamonds, Cx:y indicates acyclic nitriles. Also shown is the structures of toluene. CO_2 indicates carbon dioxide.

Skeleton 7162 ?Male 26-35 years control sample (+biog) (calculus: 1.45 mg)

The pyrolysis-GC-MS TIC revealed carbon dioxide as the major component, with significant amounts of alkenes and alkanes (Fig. 2.7). These were dominated by C_7 to C_{18} *n*-1-alkenes and *n*-alkanes, typical of unsaturated and saturated fat/oil-derived acyl lipids (Buckley et al., 1999; Hardy et al., 2012). These provide molecular evidence for a polymeric/bound acyl lipid source. However, in addition to *n*-1-alkenes and *n*-alkanes, typical of fat/oil derived lipids, the pyrogram also displayed a series of C_{10} to C_{16} 2-methyl *n*-1-alkenes and 2-methyl *n*-alkanes, presumably deriving from the branched fatty acids which are significant components of bacterial triglycerides.

There were components identified in the pyrolysate TIC which can be indicative of proteinaceous material (Hardy et al., 2012; Simmonds, 1970). These include toluene, styrene, pyridine, pyrrole, C_1 alkyl pyrroles, benzyl nitrile (phenylacetonitrile), indole and 3-methylindole (skatole) (Hardy et al., 2012; Simmonds, 1970) identified this is likely to be the main origin of these compounds in this sample, suggesting to an appreciable protein-derived component (Hardy et al., 2012; McCobb et al., 2001), although the presence of bacterial markers means the possibility that at least a partial origin could be microbial cannot be excluded. However, taken together, the presence of toluene, styrene and benzyl nitrile can indicate the amino acid phenylalanine (Stankiewicz et al., 1997, 1996) . In addition, indole and 3-methylindole (skatole) are consistent with a tryptophan amino acid source (Fuentes et al., 2010; Stankiewicz et al., 1997, 1996). This is also corroborated by the presence of aliphatic nitriles (carbon numbers *n*-$C_{14:0}$, *i*-$C_{16:0}$, *n*-$C_{16:1}$, *n*-$C_{16:0}$ (max), *i*-$C_{17:0}$, *n*-$C_{17:0}$, $C_{18:1}$, $C_{18:0}$, $C_{20:1}$ and $C_{20:0}$) suggesting a lipid (fat/oil) in this sample which has combined with protein-derived nitrogen to produce these moieties (Buckley et al., 1999). The presence of carbon dioxide is also consistent with both a lipid and amino acid/protein component in this sample. The thermally-derived carbohydrate marker 2-methyl-2-cyclopenten-1-one was identified as a trace constituent and is indicative of the original polymeric carbohydrate source (e.g. starch) (McCobb et al., 2001). No higher alkyl aromatics typically observed in soils were detected (Fuentes et al., 2010). Despite the use of mass chromatograms specifically searching for nicotine and polynuclear aromatic hydrocarbons (PAHs) (the latter group of compounds indicative of combustion processes) these were not

detected. It is possible that SIM monitoring specifically for nicotine and PAHs may detect their presence as very minor/trace constituents in future studies.

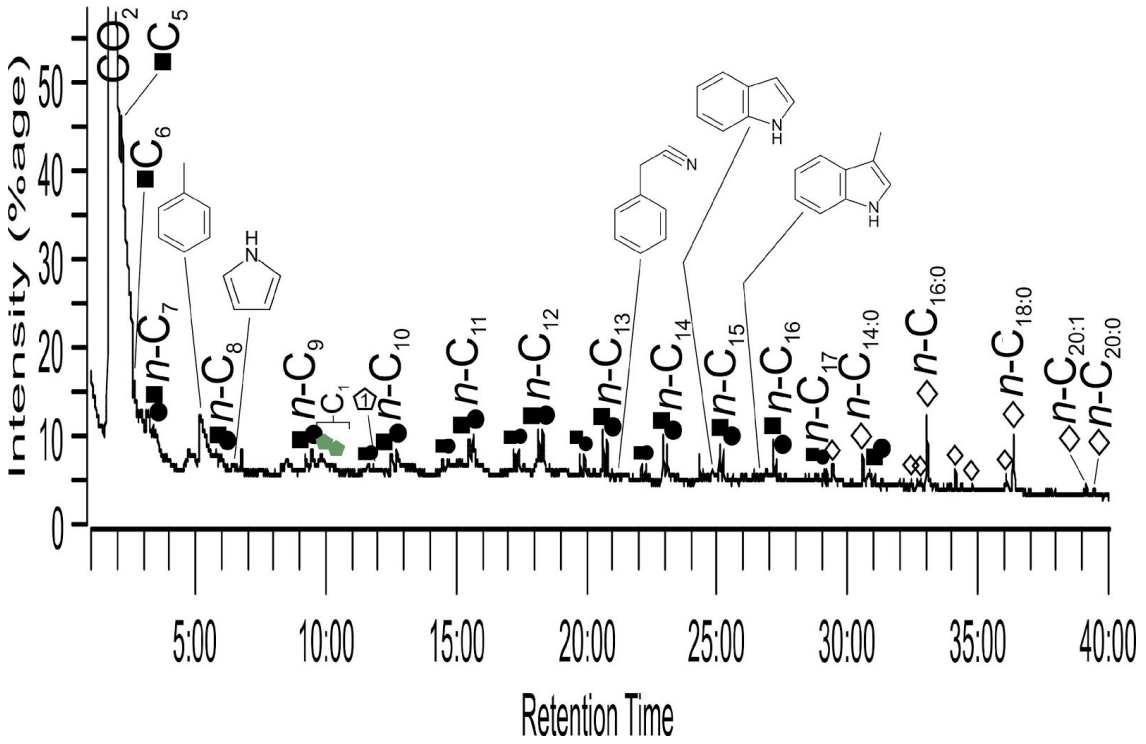

Figure 2.7 Reconstructed total ion chromatogram of the pyrogram (pyrolysis profile) (610 °C for 10s) of sample 7162. Key to Fig. 2.7: Peak identities (x indicates carbon chain length): filled squares, Cx indicates alkenes; filled circles, Cx indicates alkanes; open diamonds, Cx:y indicates acyclic nitriles; green filled pentagons indicates alkyl pyrroles (with alkyl chain length above, Cx); open pentagon with numeral inside indicates carbohydrate pyrolysis marker, 1 is 2-methyl-2-cyclopenten-1-one. Also shown are the structures of five aromatic compounds identified: toluene, pyrrole, benzyl nitrile, indole and 3-methylindole (skatole). CO_2 indicates carbon dioxide.

2.2 Chemical Analysis Summary

Ten samples of dental calculus taken from ten individuals from New Churchyard, Broadgate, were analysed by sequential thermal desorption-gas chromatography-mass spectrometry (TD-GC-MS) and pyrolysis-gas chromatography-mass spectrometry (Py-GC-MS). The results revealed a moderate amount of organic material in six of the ten samples possibly reflecting prevailing environmental conditions for biomolecular preservation. The results revealed not only evidence of bacterially-derived components as one might expect from material taken from the

microbially active human mouth, but also evidence for food-based fats and proteins, although notably there was no chemical evidence for smoke inhalation, tobacco use or cooking.

2.3 Chemical Analyses References

Buckley, S.A., Stott, A.W., Evershed, R.P., 1999. Studies of organic residues from ancient Egyptian mummies using high temperature-gas chromatography-mass spectrometry and sequential thermal desorption-gas chromatography-mass spectrometry and pyrolysis-gas chromatography-mass spectrometry. *Analyst* 124, 443–452.

Fuentes, M., Baigorri, R., González-Vila, F.J., González-Gaitano, G., García-Mina, J.M., 2010. Pyrolysis-gas chromatography/mass spectrometry identification of distinctive structures providing humic character to organic materials. *J. Environ. Qual*. 39, 1486–1497.

Hardy, K., Buckley, S., Collins, M.J., Estalrrich, A., Brothwell, D., Copeland, L., García-Tabernero, A., García-Vargas, S., de la Rasilla, M., Lalueza-Fox, C., Huguet, R., Bastir, M., Santamaría, D., Madella, M., Wilson, J., Cortés, A.F., Rosas, A., 2012. Neanderthal medics? Evidence for food, cooking, and medicinal plants entrapped in dental calculus. *Naturwissenschaften* 99, 617–626.

McCobb, L.M.E., Briggs, D.E.G., Evershed, R.P., Hall, A.R., Hall, R.A., 2001. Preservation of Fossil Seeds From a 10th Century AD Cess Pit at Coppergate, York. *J. Archaeol. Sci*. 28, 929–940.

Simmonds, P.G., 1970. Whole microorganisms studied by pyrolysis-gas chromatography-mass spectrometry: significance for extraterrestrial life detection experiments. *Appl. Microbiol*. 20, 567–572.

Stankiewicz, B.A., Hutchins, J.C., Thomson, R., Briggs, D.E.G., Evershed, R.P., 1997. Assessment of bog-body tissue preservation by pyrolysis-gas chromatography/mass spectrometry. *Rapid Commun. Mass Spectrom*. 11, 1884–1890.

Stankiewicz, B.A., van Bergen, P.F., Duncan, I.J., Carter, J.F., Briggs, D.E.G., Evershed, R.P., 1996. Recognition of Chitin and Proteins in Invertebrate Cuticles Using Analytical Pyrolysis/Gas Chromatography and Pyrolysis/Gas Chromatography/Mass Spectrometry. *Rapid Commun. Mass Spectrom.* 10, 1747–1757.

3. Microscopic Analysis

Microscopic analysis and report preparation by Anita Radini

3.0 Microscopy Summary

Twenty samples of human dental calculus, also known as tartar, were submitted for a microscopy study, in order to asses remains that may had become entrapped in its matrix, providing insights into food consumption and living conditions experienced by the examined past population. Micro remains retrieved and identified during the pilot study shows that staple food plants consisting with oats, wheat and legumes were consumed across the population. While a number of pollen grains form potential medicinal plants, such as borage, artemisia and mauve were also found. Five individuals had remains of feather barbules, thought to be chicken, probably present in dust in the environment as result of consumption or plucking of such birds. Non-dietary evidence consisted mainly with fibres of plant origin, likely flax or hemp, and animal origin consisting with wool. Such finds could be the result of exposure to occupational dust. One individual had remains of fibre that could be silk, but such finds are under investigation. Evidence of exposure to smoke and soot were also scattered across the population with one individual showing a very high concentration of micro-charcoal. Finally, due to the amount of particles retrieved in some individuals, a portion of the particles remains to be identified.

3.1 Introduction

Dental calculus microscopy studies are increasingly popular in the discipline of Archaeology, for its potential to provide information about the consumption of plant foods where other lines of evidence are lacking (Power et al, 2015). Although diet has been the main focus of recent dental calculus research, a small number of studies have in fact demonstrated that a range of micro-debris of non-dietary origin and chemical compounds can become entrapped in the calculus. For instance, smoke, occupational dust generated by pottery making and plant fibres, such as cotton (Gossypium spp.), have been recovered from the calculus matrix of past populations (Blatt et al., 2011; Blondiaux and Charlier, 2008; Hendy et al., 2014; Radini, Nikita and Shillito, 2016). In this report, dental calculus evidence is approached as an atypical environmental deposit to assess variety of debris of both dietary and non-dietary origin to which the selected individuals were exposed during life.

3.2 Materials and Methods

Twenty skeletons were sampled for dental calculus for this report, which forms part of a larger study (see Speller and Buckley this report). A small quantity of calculus was removed from the teeth using disposable stainless steel sterile blades. In order to study micro-debris entombed in the calculus matrix, such deposit needs to be dissolved. The analysis is therefore destructive. Furthermore, the scanning of slides for such study is a time consuming process. To minimize the loss of material and maximize the efficiency of the study, sub-samples of 4 mgs in weight were prepared and analysed microscopically for the pilot study. Laboratory procedures followed the protocol described in detail by Warinner *et al*. (2014) and Radini, Nikita and Shillito (2016) and summarized briefly below:

1) the calculus was washed and the external facets dissolved in HCl of low molarity to remove surface contaminants or cleaned with an acupuncture needle where necessary.
2) The 'clean' calculus was then dissolved in HCl of low molarity in a sterile tube.
3) The debris freed from the calculus was siphoned out with an Eppendorf pipette until no residue was left.
4) The retrieved remains were mounted on a glass slide in a 50:50 solution of glycerol and ultrapure water.
5) The slide was then observed under low (x200) and high magnification (x400 and x630) using a Zeiss compound microscope.
6) Debris was identified and quantified wherever possible

The identification of the micro-fossils retrieved was based on anatomical and optical properties, followed by visual comparisons with a modern reference collection. Furthermore, comparison with published material was also possible (e.g. Torrance and Barton, 2006; Petraco and Kubic 2003; Torrence and Barton 2006; Warinner *et al*. 2014). The above steps are standard procedure for the identification of both modern and ancient micro-remains. Classification and nomenclature follow Stace (1997). It must be stressed that all the categories and typologies of remains found in this study have been successfully identified by the author in other peered reviewed published work (eg Radini et al, 2016).

3.3. Microscopic Results and Discussion

The analysis of human dental calculus yielded a variety of micro debris, of both dietary and non-dietary origin. Starch granules, micro-charcoal and soot were ubiquitous across the samples, however a variety of fibres, pollen grains and other debris was also found. Results of the analysis are recorded in Table 3.1. Results are presented and briefly discussed by category of remains (erg. Starch granules, pollen, etc.).

3.3a Starch granules

Starch granules was found in all samples, and belonged to staple food crops. Morphologies of starch granules were both simple starch granules and compound ones:

- Bimodal starch granules: large sub-oval starch granules, up to 40 microns in lenght (known as type A) associated with small round starch granules, never larger then 10 microns (known as type B). Bimodal starches are known to belong to the tribe Triticeae, that of barley, rye and wheat; all are staple crops in Medieval and Post Medieval Periods diet (Banham 2004; Radini et al., 2016).

- Very interesting was the retrieval in all the skeletons of starch granules with a distinctive kidney shape, and long central hilum. Such starch granules are known to belong to the tribe Fabeae, legumes (Warinner et al. 2014), potentially species field/broad beans and vetches (Vicia spp.) Such remains are considered crops with lower archaeological visibility than cereals (Hall 2001), making these almost ubiquitous finds, a very important one.

- Compound starch granules, consisting with sub-polyhedral starch granules strictly associated one another to form a granular oval structure, and likely belonged to species of oats (Avena spp.). Oats often infested fields in the past and it was likely to have been left undisturbed and eaten together with the cultivated crops (Banham, 2004).

Finally a number of starch granules were very damaged and their nature as starch could not be confirmed.

3.3b Pollen grains

Pollen grains were found scattered across almost all individuals (see Table 3.1). Pollen of arboreal species was low in number and consisted with birch (*Betula* sp.), a tree that has several

uses for humans and that is also wind pollinated, so its pollen would be very common in the environment and many pathways for its inclusion in dental calculus are possible.

Of particular interest were pollen grains of bee pollinated and medicinal/herbal plants. Pollen grains of borage (Boraginaceae family), rose Family (Rosaceae), mauve (*Malva* sp.). and mugworts (Artemisia sp) were scattered across the individuals. Sk7982 yielded 10 pollen grains Boraginaceae, very likely borage *(Borago offciinalis L.*) and sk7162 had 7 pollen grains of mauve (*Malva* sp.), and in such quantity these remains are very likely the result of the consumption of such species for medicinal purposes, as their pollen would not be common in the environment. It must also be stressed that all species found, including birch, are commonly found in the pollen load of honey which, before the introduction of sugar, was the main form of sweetener (Crane 1984), and so honey consumption could also be a possibility.

3.3c Fibers of plant and animal origin

Non-dietary debris recovered was consisting with bast fibres, potential flax (cf. *Linum usitatissimum* L.) and/or hemp (cf. *Cannabis sativa* L.). The bast fibres of plant origin were identified upon the presence of a lumen (often narrow, as in flax) and dislocation bands along the fibre. Optical properties are normally used for their identification in forensic contexts (Petrarco and Kubic, 2003), but they are not reliable in the highly mineralized calculus matter. Fragments of fiber with distinctive scale patterns were identified as wool (*Ovis* sp.). Skeleton 1616 had higher amount of plant fibres compared to others, and skeleton 8198 had a larger amount then normal of wool fibre. Such individuals could have been involved in activities, such as textile work, where debris generated by the fibres would be in high concentration. Finally individual 8147 had 2 fragments of an unidentified fibre, this appeared very thin and smooth and could be consistent with silk, but such identification needs to be confirmed and it must be taken with caution. Plant fibres in high quantity in the environment are known to be respiratory irritants.

Table 3.1 Results of microscopic analysis of dental calculus samples

Skeleton	Triticeae st	Fabeae st	Aveneae st	Boraginaceae pl	*Malva* sp. pl	*Betula* sp. pl	Rosaceae pl	Artemisia sp. pl	cf. Linum/Cannabis sp. fb	Microcharcoal	Lepidoptera sc	Insect/Arcnida frg	Ovis sp. fb	Galliformes ftbr	Silk? Fb	Soot	Mineral grit	Undiagnostic pl tis	Unidentified	Total
175	2	16	2							86		1	1			xx	x	x	x	108
272	2	14	17				2			3		1		1		x	x	x	x	40
420	9	14	17				1			6	2	1				x	x	x	x	50
592	6	11	8						1	4				1		x	x	x	x	31
807	12	9	12			1				4	1					x	xx	x	x	39
1616	13	3	3						23	2						x	x	x	x	44
4307	22	13	4		1					8	1		1			x	x	x	x	50
5218	5	6	12			1				21			1			xx	x	x	x	46
5396	4	14	12	11						23	1	1		1		x	x	x	xx	67
5586	11	13	12			1		4		1	1					x	x	x	x	43
7162	21	8	5		7					2	1					x	x	x	x	44
7589	4	8	11	4					1	2	1			1		xx	x	x	x	32
7982	6	21	4	10		3			1	3		1				x	xxx	x	x	49
8097	13	3	12							2	1					x	xxx	x	x	31
8103	12	12	13			7	1			23			1			x	x	x	x	69
8105	2	15	6			1				2						x	x	x	xx	26
8147	6	2	12			1				25				1	2	x	x	x	x	49
8198	5	1	4					1		11			13			x	x	x	x	35
8204	12	8	9				3			1		1				x	x	xx	x	34
8223	3	12	16							25	1					x	x	x	x	57

Note: st indicates starch; pl indicates pollen; fb indicates fibre

3.3d Microcharcoal, Soot and mineral grit

All individuals in this study had a variable amount of micro-charcaol and soot entombed in their calculus matrix. Charcoal and soot could be the result of exposure to smoke for heating purposes or potentially due to sanitation of the environment, but they could also be the result of the ingestion of smoked/roasted food. Although such remains were found in all individuals, skeleton

175 had a very large amount of charcoal fragment and soot, and this could be an identification of exposure to such pollutants as result of unhealthy living condition or as result of an occupation that required the burning of large quantity for fuel.

3.3e Other remains

Five individuals had a very low amount of feather barbule fragments, which were consistent with those of the Galliformes order of birds following Dove and Koch (2011), and are most likely to be fragments of chicken downy feather barbules. Such remains are very small and light and tend to remain airborne for long period of time. These could be accidental ingested on inhaled during oral breathing if present in the environment. Mineral grit was also present in all calculus samples, and could be accidently ingested in food, for example from the quern stones used to process cereal crops.

3.3f Unidentified debris

A number of remains could not be identified, and will be subject of further analysis. However, it was possible to separate debris of plant origin upon the visible presence of plan cell wall, and such remains are thought to be the result of the consumption of leafy greens vegetables such as cabbage, a staple in the diet during the later medieval period (Hall 2001). Leafy crops that may have been cooked for long period of time do not have features that allows their identification.

3.4 Conclusions and future direction

The analysis yielded evidence of staple plant food, some with low archaeological visibility. Potential occupational and environmental dust was also found. Finally, soot and charcoal were ubiquitous across the assemblage, suggesting exposure to smoke and other potential respiratory irritants, such as fibers from plants perhaps of occupational origin. Further work on the remains is currently in progress to implement the identification of debris and to confirm the nature of some of the remains as occupational dust.

3.5 Microscopic References

Banham, D. (2004). *Food and drink in Anglo-Saxon England*. Stroud, Gloucestershire: Tempus

Blatt, S., Redmond, Br., Cassman, V. and Sciulli, P. (2011). Dirty teeth and ancient trade: Evidence of cotton fibres in human dental calculus from Late Woodland, Ohio, *International Journal of Osteoarchaeology, 21* (2011), pp. 669-678

Blondiaux, J. and Charlier, P. (2008).Palaeocytology in skeletal remains: microscopic examination of putrefaction fluid deposits and dental calculus of skeletal remains from French archaeological sites'. *International Journal of Osteoarchaeology*, 18 (2008), pp.1–10

Crane, E., (1984). *The Archaeology of Beekeeping.* London: Duckworth

Dove, C.J. and Koch, S.L. (2011). Microscopy of feathers: a practical guide for forensic feather identification. *Microscope-Chicago*, *59*(2), p.51.

Dyer, C. (2006). Gardens and garden produce. In C. M. Woolgar, D. Serjeantson and T. Waldron (eds.), *Food in medieval England. Diet and nutrition* Oxford University Press, Oxford pp. 27-40.

Hall, A. (2000) A Brief History of Plant Food in the City of York. In White, E (Ed.) *Feeding a City: York*, Devon: Prospect Books, pp. 23-41.

Hendy, J., Charlton, S. and Radini, A. (2013) Ancient Human Dental Calculus: an unexpected journey into the past *The Post Hole*. http://www.theposthole.org/read/article/20

Petraco, N. and Kubic, T. (2003) Color atlas and manual of microscopy for criminalists, chemists, and conservators. New York: CRC Press

Radini, A., Nikita, E., Shillito (2016). Human Dental Calculus in a Medieval Urban Environment In: B. Jervis, L. Broderick and I. Grau B. (eds) *Everyday Life in Medieval Europe: Environmental and Artefactual Approaches to Dwelling in Town and Country'* Brepols.

Stace, C. (1991). *New Flora of the British Isles*. Cambridge University Press.

Torrence, R. and Barton, H. (2006) *Ancient Starch Research*. California: Left Coast Press Inc.

Warinner, C., Rodrigues, J., Vyas, R., Christian Trachsel, C., Shved, N., Grossmann, J., Radini, A., Hancock, Y., Tito, R. Y., Fiddyment, Camilla Speller, C., Hendy, J., Charlton, S., Luder, H. U., Salazar-García, D. C.,Eppler, E., Seiler, R., Hansen, L., Samaniego Castruita, J., A., Barkow-Oesterreicher, S., Teoh, K. Y., Kelstrup, C., Olsen, J. V., Paolo Nanni, P., Kawai, T., Willerslev, E., Christian von Mering, C., Lewis, C. M. Jr., Collins, M. J., Thomas, P., Gilbert, P., Rühli, F., Cappellini, C., (2014). 'Pathogens and host immunity in the ancient human oral cavity' *Nature Genetics* 46(4), 336-344.